International Journal of Computer Vision 21(3), 223–247 (1997)

On the Geometry of Visual Correspondence

CORNELIA FERMÜLLER AND YIANNIS ALOIMONOS
Computer Vision Laboratory, Center for Automation Research, University of Maryland, College Park, MD 20742-3275; and Computational Vision and Active Perception Laboratory, Royal Institute of Technology, S-100 44 Stockholm, Sweden

Received March 1, 1994; Revised January 5, 1995; Accepted May 30, 1995

Abstract. Image displacement fields—optical flow fields, stereo disparity fields, normal flow fields—due to rigid motion possess a global geometric structure which is independent of the scene in view. Motion vectors of certain lengths and directions are constrained to lie on the imaging surface at particular loci whose location and form depends solely on the 3D motion parameters. If optical flow fields or stereo disparity fields are considered, then equal vectors are shown to lie on conic sections. Similarly, for normal motion fields, equal vectors lie within regions whose boundaries also constitute conics. By studying various properties of these curves and regions and their relationships, a characterization of the structure of rigid motion fields is given. The goal of this paper is to introduce a concept underlying the global structure of image displacement fields. This concept gives rise to various constraints that could form the basis of algorithms for the recovery of visual information from multiple views.

1. Introduction

The recovery of the structure of a scene from multiple views and the transformation between the views has been studied in the context of several visual tasks. Indeed, the problems of stereo, 3D motion estimation, calibration, obstacle detection, pose estimation for recognition, etc., can be regarded as special instances of the general recovery problem (Bergholm, 1988; Daniilidis, 1992; Daniilidis and Nagel, 1990; Faugeras, 1992; Faugeras et al., 1987; Faugeras, and Papadopoulo, 1993; Gårding et al., 1993; Koenderink and Doorn, 1991; Navab et al., 1993; Nelson and Aloimonos, 1988; Tistarelli and Sandini, 1992; Ullman, 1979; Ullman and Basri, 1991). Approaches to various aspects of this problem that have appeared in the literature seek a solution in two computational steps. First, a description that relates local measurements in multiple views is developed; local descriptors include stereo disparity measurements, motion disparity measurements, motion fields, partial disparity fields such as those along the X- or Y-axes, or normal motion fields (the projections of motion fields along the gradient direction) (Anandan and Weiss, 1985; Hildreth, 1984; Horn and Schunck, 1981; Koenderink, 1986; Shulman and Hervé, 1989). Second, knowledge of the model of the geometric transformation between the multiple views provides constraints on the local descriptors; these constraints are used to relate image measurements to the 3D scene and viewing geometry (Faugeras and Maybank, 1990; Horn, 1990; Koenderink and van Doorn, 1991; Liu and Huang, 1988; Maybank, 1993; Prazdny, 1980; Spetsakis and Aloimonos, 1988; Tsai and Huang, 1984).

This paper deals with the case where the transformation between the views is described by a rigid motion. The rigid motion model imposes constraints on the local image measurements (disparity measurements, optical flow field, normal flow field), which thus have a certain global structure. The goal of this study is to make explicit aspects of this structure that are due only to rigid motion.

In the remainder of this paper we will use the terms motion vector and motion field to refer to the 2D image displacements (local descriptors), and normal motion vector or normal motion field to refer to the motion vector components along the image gradients.

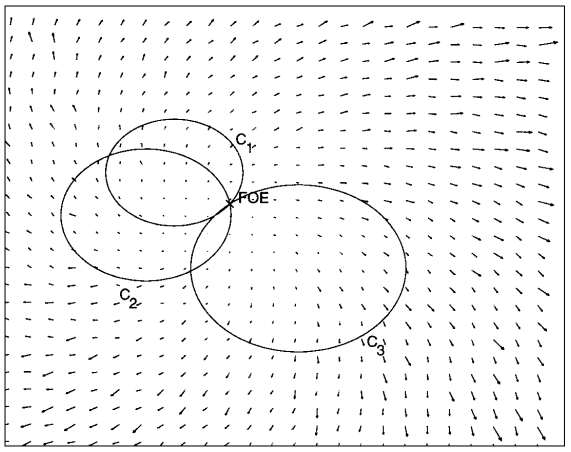

Figure 1. The rigid motion constrains the motion vectors to lie on conic sections in the image plane. C_1, C_2 and C_3 are curves containing the motion vectors of values (0.5, 0.5), (0.1, 0.7), and $(-0.4, -0.4)$.

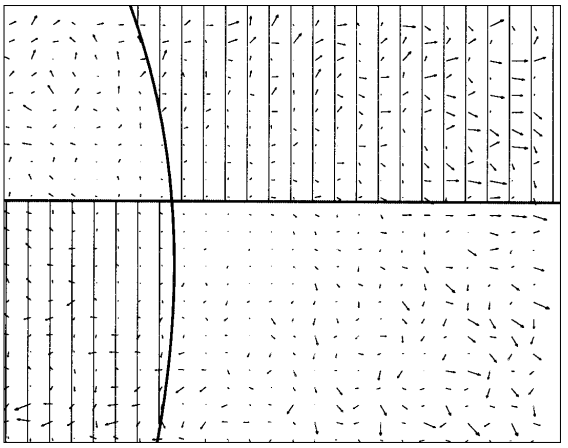

Figure 2. For a normal motion field all vectors of certain value are constrained to lie within regions. The boundaries of these regions depend on the 3D motion.

1.1. What is to Come

Before we proceed, in order to provide the reader with an intuitive notion of the the global structure of rigid motion fields, which is the subject of this study, we present in Figs. 1 and 2 two simple examples. Figure 1 shows a motion field generated by an observer moving rigidly with regard to some surface. The analysis in this paper will show that the rigid motion, independently of the scene in view, constrains the locations of the motion vectors that have certain values. For example, all vectors ($u = 0.5$, $v = 0.5$) lie on the conic section C_1. (This does not mean that all vectors on C_1 have motion vector (0.5, 0.5); it means only that if there exists in the image a point with motion vector equal to (0.5, 0.5), this point will lie on the curve C_1.) Similarly, curves C_2 and C_3 contain all points with motion vectors (0.1, 0.7) and $(-0.4, -0.4)$ respectively. This study investigates properties of the classes of curves which are loci of points where the motion vector has some property. For example, we will show that all curves corresponding to vectors of fixed value intersect in one point whose coordinates encode information about the translational component of the motion, i.e., the FOE.

Figure 2 shows a normal motion field (i.e., the component of the motion vector along the image gradient at every point) resulting from the same rigid motion. Points in the image plane where the normal motion vector can have a particular length and direction are clustered in regions whose boundaries depend on the 3D motion. To illustrate this in Fig. 2 all normal motion vectors parallel to the Y-axis and of length 0.3 are shown to be in the area marked by vertical lines. We will study the relationships of such areas to each other and to the curves described above. For example, we will see that the intersection of the region boundaries provides the parameters of the translation as well as the rotation of the underlying 3D motion.

The main goal of this paper is to reveal global geometric aspects of flow or displacement fields which are due to rigid motion. In this sense this study is related to a small number of previous studies, which were concerned with a global decomposition of motion fields for the specialized cases of pure translation (Jain, 1983; Horn and Weldon, 1987) and pure rotation (Aloimonos and Brown, 1984). In earlier work (Fermüller, 1993; Fermüller and Aloimonos, 1994) we dealt with the general case and described certain global properties of rigid normal motion fields manifested as patterns defined on the sign of subsets of the motion vectors. In this paper we formulate a more general framework having in mind to investigate global structures through the study of functions of the the values of 2D rigid displacement fields. This is achieved by defining functions on the vectors of the flow field and studying the location of the level sets of these functions. The functions employed here are of a simple nature. In particular, we concentrate on optic flow vectors of constant value, normal flow vectors of constant value, and on certain linear and quadratic functions defined on the normal flow, and we also relate this analysis to our earlier results.

The remainder of this paper is divided in three parts. The first part (Sections 2 and 3) is devoted to the

analysis of rigid motion fields, the second part (Section 4) is concerned with rigid normal motion fields, and in the last part (Section 5) applications to a variety of visual tasks using the theoretical results, are outlined. In particular, Section 2 describes the well-known equations relating the image motion field to the 3D motion for the case of a planar retina, and Section 3 explains the structure of the "iso-motion curves" and gives an analysis of the relationships between different iso-motion curves. An iso-motion curve $C_{\mathbf{u}}$ is a locus of points where the vector field representing the image motion could take on a fixed value defined in terms of $\mathbf{u}$. Analogously, when dealing with normal flow, we encounter "iso-normal motion regions". Section 4 studies the relationship between such regions and the 3D motion parameters. The concept of selecting vectors of certain lengths and directions is extended to certain vector valued functions. In the section on applications, we discuss how the concepts and structures introduced in the paper could serve as the basis for a variety of perceptual mechanisms underlying visual tasks. The advantage of the constraints developed is due to the fact, that they are defined globally on the image, as they relate motion measurements from different parts of the image to each other. The globality gives the constraints the potential of being exploited in tasks related to the recovery of the parameters describing the rigid motion configuration. They may be used in algorithms computing the extrinsic as well as the intrinsic parameters of a rigid motion configuration or stereo setting. They also may be exploited to verify that a vector field is only due to rigid motion and to locate areas in the image where this constraint does not hold—for example, in the detection and localization of independently moving objects for a moving observer. In general, they could be utilized whenever navigational problems are addressed that involve estimating aspects of 3D motion, such as image stabilization, servoing, or docking. Finally, the appendix develops the equivalent of the iso-motion contours and the iso-normal motion regions on the sphere, thus providing a simple geometric intuition to these concepts.

2. Localization of Motion Measurements

The 2D motion field on an imaging surface is the projection of the 3D motion field of the scene points moving relative to that surface. If this motion is rigid, it is composed of a translation $\mathbf{t}$ and a rotation $\boldsymbol{\omega}$. For the case of a moving camera in a stationary environment each scene point $\mathbf{R} = (X, Y, Z)$ measured with respect to a

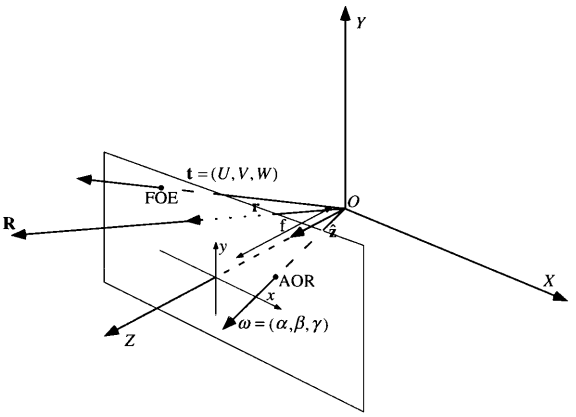

Figure 3. Image formation using perspective projection on a planar retina.

coordinate system $OXYZ$ fixed to the camera moves relative to the camera with velocity $\dot{\mathbf{R}}$, where

$$\dot{\mathbf{R}} = -\mathbf{t} - \boldsymbol{\omega} \times \mathbf{R}. \tag{1}$$

Projecting the 3D motion vectors on a retina of a given shape gives the image motion field.

If the center of projection is at the origin O and the image is formed on a plane orthogonal to the Z-axis at distance f (focal length) from the nodal point (see Fig. 3), the relation between the image point $\mathbf{r} = (x, y, f)$ and the scene point $\mathbf{R}$ under perspective projection is

$$\mathbf{r} = \frac{f}{\mathbf{R} \cdot \hat{\mathbf{z}}}\mathbf{R},$$

where $\hat{\mathbf{z}}$ is a unit vector in the direction of the Z-axis and the "$\cdot$" denotes the inner product of vectors.

If we now differentiate $\mathbf{r}$ with respect to time, and substitute for $\dot{\mathbf{R}}$, we obtain the following equation for $\dot{\mathbf{r}}$:

$$\dot{\mathbf{r}} = \frac{1}{\mathbf{R} \cdot \hat{\mathbf{z}}}((\mathbf{t} \cdot \hat{\mathbf{z}})\mathbf{r} - f\mathbf{t}) - \frac{1}{f}[\mathbf{r}\boldsymbol{\omega}\hat{\mathbf{z}}]\mathbf{r} - \boldsymbol{\omega} \times \mathbf{r}, \tag{2}$$

where $[\mathbf{r}\boldsymbol{\omega}\hat{\mathbf{z}}] = \mathbf{r} \cdot (\boldsymbol{\omega} \times \hat{\mathbf{z}})$ (triple product).

The first term for $\dot{\mathbf{r}}$ in Eq. (2) denotes the translational motion component which depends on the depth $Z = \mathbf{R} \cdot \hat{\mathbf{z}}$, while the second term denotes the rotational component which does not depend on depth, but only on the three rotational parameters. As can be seen from the equations, using perspective projection, only the scaled translation $\frac{\mathbf{t}}{Z}$ can be recovered. The points where the axis of translation pierces the retina are called the Focus of Expansion (FOE) in the case of positive

translation along the Z-axis or Focus of Contraction (FOC) otherwise, since at these points the translational motion components are zero and all translational motion vectors point away from or towards these points. Similarly, we call the point where $\boldsymbol{\omega}$ (the rotation axis) pierces the retina the Axis of Rotation point (AOR). At this point the rotational motion is zero.

We are concerned with how the fact that the motion is rigid constrains the image motion vector field. Looking at a single measurement, we see that due to rigidity the motion vector at every point is constrained to lie in a one-dimensional subspace (defined by the rotational component and a translational component of which we know the direction but not the length). Since the distance from the scene to the image is positive, the possible space for the motion vector at every point is further reduced to a half-space.

In order to separate the constraints on the motion field due to shape from those due to motion, we take the approach of studying answers to the following questions: Given a certain value $\mathbf{v}(\mathbf{p})$ for a motion vector at point $\mathbf{p}$ (or a vector valued function), where are the locations $\mathbf{p}$ on the retina, for which the motion vector $\dot{\mathbf{r}}$ at $\mathbf{p}$ (hereafter $\dot{\mathbf{r}}(\mathbf{p})$) could take the value $\mathbf{v}(\mathbf{p})$? These concepts are explored below.

3. Iso-Motion Contours in the Plane

3.1. *Characterization of the Form of Iso-Motion Contours in the Plane*

If the scene is projected on a planar retina the image velocity field is given by Eq. (2). We express this equation in the more common component notation: $\dot{\mathbf{r}} = (\dot{r}^1, \dot{r}^2, \dot{r}^3)$. $\dot{r}^3$ is always zero. We denote $\dot{r}^1$ by u and $\dot{r}^2$ by v, $\mathbf{t} = (U, V, W)$, $\boldsymbol{\omega} = (\alpha, \beta, \gamma)$. If we introduce new coordinates for the direction of translation $(x_0, y_0) = (\frac{Uf}{W}, \frac{Vf}{W})$, we obtain the well-known equations (Longuet-Higgins and Prazdny, 1980)

$$\begin{aligned} u &= u_{\text{trans}} + u_{\text{rot}} \\ &= (-x_0 + x)\frac{W}{Z} + \alpha\frac{xy}{f} - \beta\left(\frac{x^2}{f} + f\right) + \gamma y \quad (3) \\ v &= v_{\text{trans}} + v_{\text{rot}} \\ &= (-y_0 + y)\frac{W}{Z} + \alpha\left(\frac{y^2}{f} + f\right) - \beta\frac{xy}{f} - \gamma x \quad (4) \end{aligned}$$

We are interested in the locus of points with motion vector $\mathbf{u} = (u, v)$. To obtain the locations (x, y) in the image plane for which the motion vector has some constant value (u, v), we bring the rotational components in Eqs. (3) and (4) to the left side and divide (3) by (4):

$$\begin{aligned} \frac{u - u_{\text{rot}}}{v - v_{\text{rot}}} &= \frac{u_{\text{trans}}}{v_{\text{trans}}} \\ \frac{u - \left(\alpha\frac{xy}{f} - \beta\left(\frac{x^2}{f} + f\right) + \gamma y\right)}{v - \left(\alpha\left(\frac{y^2}{f} + f\right) - \beta\frac{xy}{f} - \gamma x\right)} &= \frac{x - x_0}{y - y_0} \end{aligned} \quad (5)$$

which results in the equation

$$\begin{aligned} \phi(x, y, u, v) = {} & y^2\left(\frac{\alpha x_0}{f} + \gamma\right) - xy\left(\frac{\beta x_0}{f} + \frac{\alpha y_0}{f}\right) \\ & + x^2\left(\frac{\beta y_0}{f} + \gamma\right) - x(\alpha f + \gamma x_0 - v) \\ & - y(\beta f + \gamma y_0 + u) + x_0(\alpha f - v) \\ & + y_0(\beta f + u) = 0 \end{aligned} \quad (6)$$

describing a second order curve in the image plane. Hereafter, we will refer to the curves given by Eq. (6) as iso-motion contours, in particular as $\mathbf{u}$ iso-motion contours $C_{\mathbf{u}}$ (or (u, v) iso-motion contours $C_{(u,v)}$) when denoting the parameterization by $\mathbf{u}$ $((u, v))$.

Since the values of u and v do not appear in the quadratic terms of Eq. (6), but only in the linear and constant terms, the nature of the curve (i.e., whether it is an ellipse, hyperbola, or parabola) is independent of u, v, and thus is the same for all such parametrized curves of a given motion field. The axes of the conics are all parallel to each other with slopes m and $\frac{-1}{m}$, where m is the positive of the two values (Selby, 1972)

$$\frac{(\beta y_0 - \alpha x_0) \mp \sqrt{(\alpha^2 + \beta^2)(x_0^2 + y_0^2)}}{(\beta x_0 + \alpha y_0)}.$$

The nature of the iso-motion contours depends on the values of the translation and rotation. Depending on the value l, where

$$l = \left(\frac{\beta x_0}{f} + \frac{\alpha y_0}{f}\right)^2 - 4\left(\frac{\alpha x_0}{f} + \gamma\right)\left(\frac{\beta y_0}{f} + \gamma\right)$$

the contour is a hyperbola if $l > 0$, an ellipse if $l < 0$, or a parabola if $l = 0$. Figures 4(a) and (b) show two classes of iso-motion curves for two different motion fields.

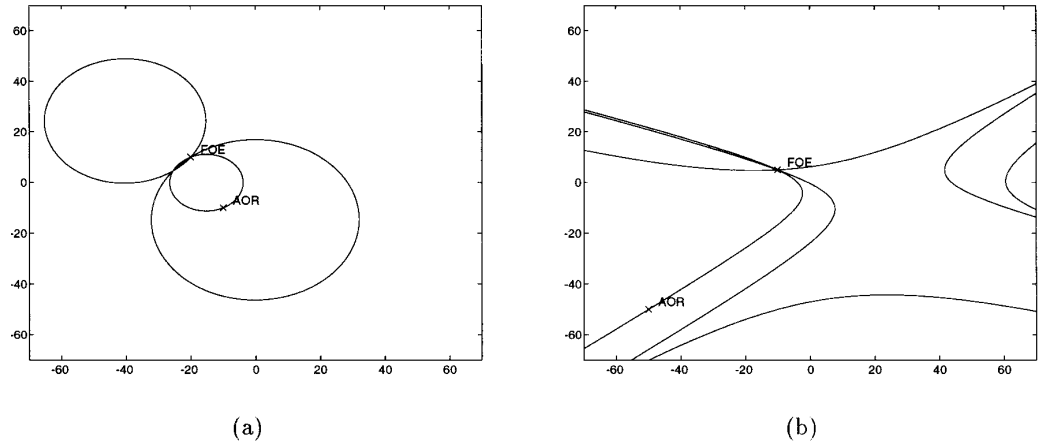

Figure 4. (a) Ellipses as iso-motion contours, (b) hyperbolas as iso-motion contours.

3.2. *The Structure of Iso-Motion Contours in the Plane*

In this section relationships between iso-motion contours in the plane are investigated. We are interested in studying the intersections of iso-motion contours and the relationship between the iso-motion contours and the possible motion measurements along these curves.

To characterize the intersections of iso-motion contours, we look at the possible values the motion vector can take at a point. For a given rigid motion the rotational component of the motion vector and the direction of the translational component have fixed values for a specific point. The only degree of freedom lies in the variability of the depth. At point $\mathbf{P}(x, y)$ the motion vector can take the value

$$\mathbf{u}(x, y) = \mathbf{u}_{\text{rot}}(x, y) + \lambda \mathbf{u}_{\text{tr}}(x, y), \tag{7}$$

where $\mathbf{u}_{\text{tr}}(x, y) = (x - x_0, y - y_0)$ and λ is the scaled depth value $\frac{W}{Z}$. The iso-motion contours that pass through $\mathbf{P}(x, y)$ have to correspond to the motion vectors given by Eq. (7), and thus every point can be considered as the intersection of the family of $\mathbf{u}(x, y)$ iso-motion contours, as defined in (7).

Let us now consider, as before, the iso-motion contours of parallel motion vectors, i.e., let us consider the iso-motion contours of values $k(u, v)$, where (u, v) is a unit vector and k a scalar $\in \Re$. These can be obtained from Eq. (6) by substituting ku for u and kv for v.

Equation (6) can be written as a sum of a quadratic expression $q(x, y)$ and a linear expression $p(x, y)$ multiplied by k:

$$\begin{aligned}
&\phi(x, y, u, v, k) \\
&\quad = q(x, y) + kp(x, y) = 0 \\
&\quad = y^2\left(\frac{\alpha x_0}{f} + \gamma\right) - xy\left(\frac{\beta x_0}{f} + \frac{\alpha y_0}{f}\right) \\
&\qquad + x^2\left(\frac{\beta y_0}{f} + \gamma\right) - x(\alpha f + \gamma x_0) \\
&\qquad - y(\beta f + \gamma y_0) + x_0 \alpha f + y_0 \beta f \\
&\qquad + k(xv - yu - x_0 v + y_0 u) = 0
\end{aligned} \tag{8}$$

Independently of k, the two intersection points of $q(x, y)$ and $p(x, y)$ are elements of all the (ku, kv) iso-motion contours $\phi(x, y, u, v, k)$. Thus the family of contours has two common intersection points. Both these points, since they lie on $\phi(x, y, u, v, k)$ for every k, also lie on the zero motion contour. Thus all families $\phi(x, y, u, v, k)$ of iso-motion contours intersect at two points on the zero motion contour (see Fig. 5). One of them is the FOE. The other one is denoted by $\mathbf{P}_{k(u,v)}$.

Since $\mathbf{P}_{k(u,v)}$ lies on all $\phi(x, y, u, v, k)$ iso-motion contours the value of the motion vector at $\mathbf{P}_{k(u,v)}$ will certainly be $k(u, v)$ for some k. Thus the direction of the motion vector for every point on the zero motion contour is defined. Since $\mathbf{P}_{k(u,v)}$ lies on the zero motion contour, and thus from Eq. (7) it follows that

$$\mathbf{u}_{\text{tr}} = \mu \mathbf{u}_{\text{rot}}$$

(i.e., the translational component is parallel to the rotational one), we find that the motion vector for every

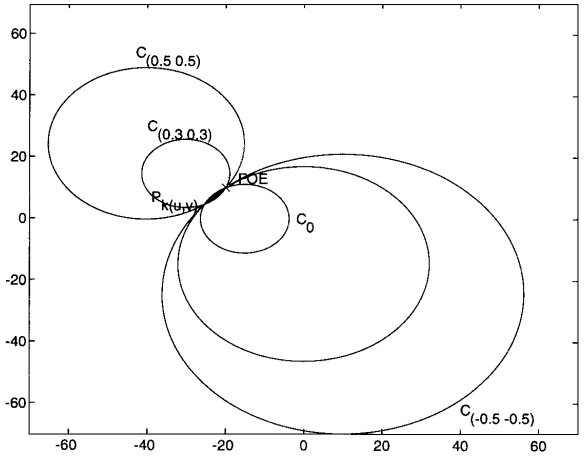

Figure 5. The family $\phi(x, y, u, v, k)$ of iso-motion contours intersect at two points on the zero motion contour: The FOE and $\mathbf{P}_{k(u,v)}$.

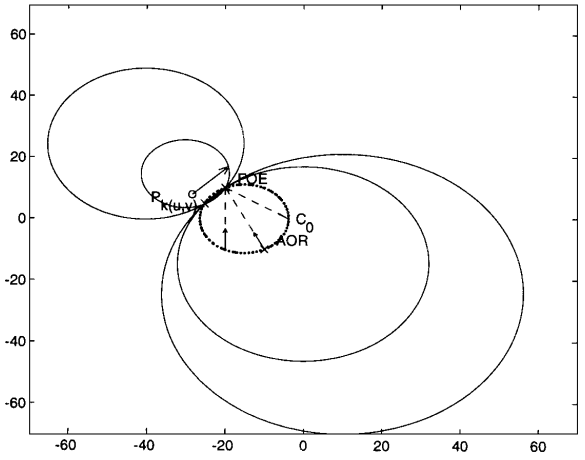

Figure 6. The motion vector in $\mathbf{P}_{k(u,v)}$ is parallel to (u, v). For every point on the zero motion contour the motion vector lies on a line connecting the point with the FOE.

point on the zero motion contour is along the direction of its translational component and thus lies on a line connecting the point with the FOE (see Fig. 6).

If we look at points on general **u** motion contours, where **u** is any 2D vector, we can make the following statement about the direction of the motion vector there. Since any point **P** is the intersection of iso-motion contours of value $\mathbf{u} + \lambda\mathbf{u}_{\text{tr}}$, if we subtract **u** from the actual motion vector **v**, we are left with a vector $\mathbf{v}_-$ which is parallel to the translational motion ($\mathbf{v}_- = \mathbf{v} - \mathbf{u} = \lambda\mathbf{u}_{\text{tr}}$) and thus lies on a line that passes through the FOE (see Fig. 7).

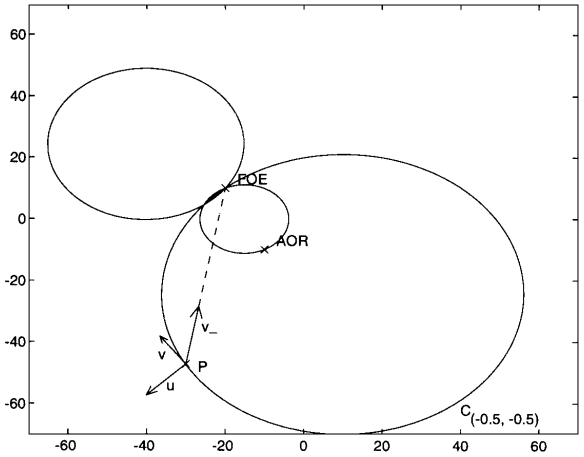

Figure 7. For any point P with motion vector **v** on a general **u** iso-motion contour the motion vectors $\mathbf{v}_-$, where $\mathbf{v}_- = \mathbf{v} - \mathbf{u}$, is parallel to the translational component **v**.

3.3. Depth Positivity

A **u** iso-motion contour is defined by Eq. (5) as the geometrical locus of points for which the direction of translation is equal to the direction of the difference between **u** and the rotational component, not considering any constraints on the depth. Since the scene lies in front of the camera, and thus an additional restriction is imposed on the values, only a part of the iso-motion contour can contain motion vectors.

Let us assume that the translation along the Z-axis has positive sign and thus $\lambda = \frac{W}{Z} > 0$. Therefore, from Eq. (7), we obtain two inequalities

$$(x - x_0)(u - u_{\text{rot}}) > 0 \tag{9}$$

$$(y - y_0)(v - v_{\text{rot}}) > 0 \tag{10}$$

These inequalities define a curve segment whose endpoints are those for which $\lambda = 0$ and $\lambda = \infty$. If $\lambda = 0$, $\mathbf{u} = \mathbf{u}_{\text{rot}}$, if $\lambda = \infty$, $\mathbf{u} = \mathbf{u}_{\text{trans}}$, which means that the curve segment connects a point $\mathbf{R}_u$ (for which the rotational motion is equal to **u**) to the FOE, the first point corresponding to infinite depth, and the second to zero depth (i.e., a scene point on the image plane). Along the curve segment the depth decreases continuously. This simple observation can give rise to qualitative techniques for the estimation of structure. In Fig. 8 two curves of a family of $k(u, v)$ iso-motion contours are displayed. The curve segments which correspond to positive depth values are marked with circles.

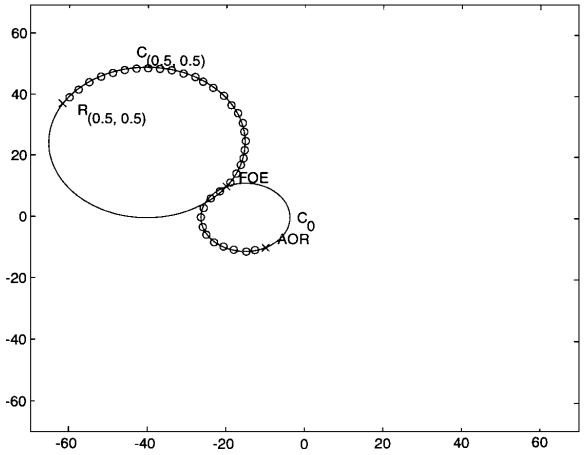

Figure 8. Two of a family of $k\mathbf{u}$ iso-motion contours (C_0 and $C_{0.5,0.5}$): The curve segments for which the depth is positive are marked by circles. The endpoints of these segments are the FOE and the points $\mathbf{R}_{k\mathbf{u}}$.

3.4. *Fixating Stereo*

The image displacement field due to binocular disparity measurements obtained by a stereo system fixating at a point deserves some separate discussion. This configuration has often been studied in the psychophysical literature (von Helmholtz, 1896). In particular, a concept that can be regarded as a special case of the iso-motion contours, has been investigated: The locus of points in space that yield zero disparity, the so-called *horopter*. For a general stereo system in fixation (see Fig. 9) the horopter consists of two intersecting curves, the first being a circle in the plane defined by the two optical axes of the two cameras passing through the two nodal points and the fixation point, and the second being orthogonal to the plane of the circle and passing through the fixation point.

Let us fix a coordinate system to the left camera and let us describe the disparity (motion) of the right camera with respect to left one. We assume that the baseline is in the XZ-plane. To obtain a unified notation, we use here the small baseline approximation in order to be able to employ the same differential equations as before. Our concern here is the study of the structure of disparity fields, and the structure itself is not affected by this assumption. The center of the right camera is in the XZ-plane and the rotation, if the two cameras fixate at one point, is only around the Y-axis. Therefore, there are only two unknown motion parameters for a fixating stereo configuration, namely x_0 and β. We thus obtain the following equation for the iso-motion contours of

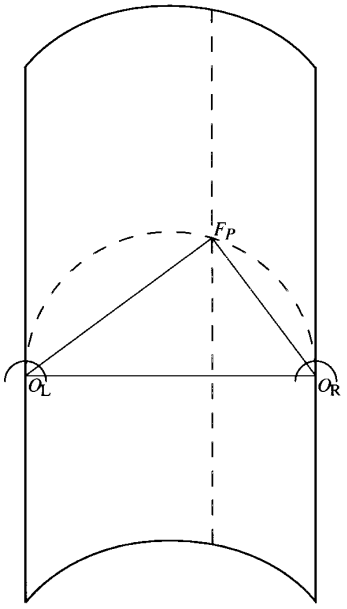

Figure 9. Binocular viewing geometry under fixation: The dotted circle through the fixation point and the eyes and the dotted line perpendicular to this circle indicate the horopter, i.e., the locus of points in 3D that yield zero disparity.

a fixating stereo in the image plane:

$$\frac{x_0}{f}\beta xy - xv_1 + y(\beta f + u_1) - x_0 v_1 = 0 \qquad (11)$$

The iso-motion contours are hyperbolas. Their axes are parallel to the medians, and the center of their axes is (Selby, 1972)

$$(x_c, y_c) = \left(\frac{(-\beta - u_1)\, f}{\beta x_0}, \frac{v_1 f}{\beta x_0}\right).$$

The zero motion contour, which is the projection of the horopter on the image plane, is defined as

$$-y\beta\left(\frac{x_0 x}{f} + f\right) = 0$$

which is the equation of two lines, one being the x-axis, the other a line parallel to the y-axis with x-coordinate $x = \frac{-f^2}{x_0}$. These lines, of course, constitute a degenerate hyperbola. The families of iso-motion contours corresponding to parallel measurements (i.e., the $k(u, v)$ iso-motion contours) have the FOE as one intersection point and as the other a point $\mathbf{P}_{k(u,v)}$ which lies on the part of the zero motion contour for which $x = \frac{-f^2}{x_0}$. Thus for every point along the line $x = \frac{-f^2}{x_0}$

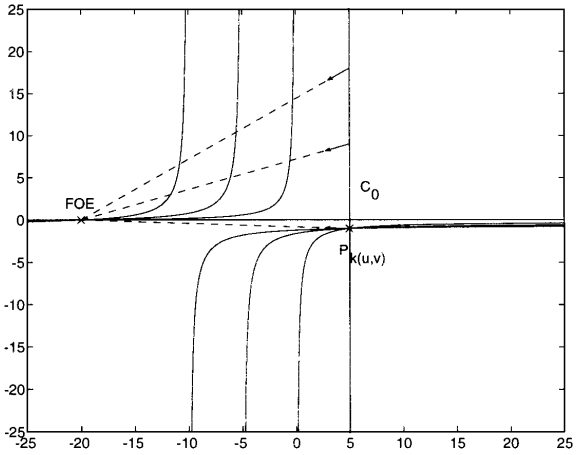

Figure 10. Iso-motion contours for fixating stereo: For all points along a line parallel to the Y-axis the motion vectors are in the direction of their translational motion components.

the direction of the flow is in the direction of the translational motion component (see Fig. 10).

4. Normal Motion Constraints

The vector field which represents the components of the motion field perpendicular to edges is referred to as the normal motion field (Aloimonos, 1990; Verri and Poggio, 1989). It is uniquely defined by local image measurements and can be derived without confronting the aperture problem. Although a normal motion field seems to contain less information than the exact motion field, the motion involved is still manifested in it. In particular, if the normal motion field is due to a rigid motion, it possesses a certain structure.

In this section we investigate the locus of points in the image plane where the normal motion vector can take on a certain value. We first deal with the case of a normal motion vector of constant value, and later generalize to certain vector-valued functions linear and quadratic in the image coordinates. It will be shown that the only constraint for the location of these image points originates from the fact that the depth has to be positive. As a result the possible locations are found to be connected areas in the image plane. The shapes of these areas are defined by the rigid motion.

4.1. Iso-Normal Motion Areas

If $\mathbf{u}$ is the motion vector at a point (x, y) and $\mathbf{n} = (n_x, n_y)$ is a unit vector in gradient direction, the normal motion $\mathbf{u_n}$ is

$$\mathbf{u_n} = (\mathbf{u} \cdot \mathbf{n})\mathbf{n}.$$

Substituting for the components of $\mathbf{u}$ from (3) and (4), we obtain u_n for the value of the vector $\mathbf{u_n}$ along the gradient direction:

$$u_n = u_{\text{rot}} n_x + u_{\text{trans}} n_x + v_{\text{rot}} n_y + v_{\text{trans}} n_y \qquad (12)$$

and thus

$$\begin{aligned} &\frac{W}{Z}((x - x_0)n_x + (y - y_0)n_y) \\ &\quad = u_n - \left(\alpha\frac{xy}{f} - \beta\left(\frac{x^2}{f} + f\right) + \gamma y\right)n_x \\ &\quad\quad - \left(\alpha\left(\frac{y^2}{f} + f\right) - \beta\frac{xy}{f} - \gamma x\right)n_y. \end{aligned} \qquad (13)$$

We are concerned with the question: Where in the image plane can the normal motion field take on a certain constant value $\mathbf{u_n}$ (i.e., where could normal motion vectors of a certain length u_n and direction (n_x, n_y) be?)? The depth has to be positive. If we assume $W > 0$, we obtain the following inequality:

$$\begin{aligned} &\left[u_n - \left(\alpha\frac{xy}{f} - \beta\left(\frac{x^2}{f} + f\right) + \gamma y\right)n_x \right. \\ &\quad \left. - \left(\alpha\left(\frac{y^2}{f} + f\right) - \beta\frac{xy}{f} - \gamma x\right)n_y\right] \cdot \\ &\qquad [(x - x_0)n_x + (y - y_0)n_y] > 0 \\ &\quad h(u_n, \alpha, \beta, \gamma, x, y) \cdot g(x_0, y_0, x, y) > 0 \end{aligned} \qquad (14)$$

$h(u_n, \alpha, \beta, \gamma, x, y) = u_n - (\alpha\frac{xy}{f} - \beta(\frac{x^2}{f} + f) + \gamma y)n_x - (\alpha(\frac{y^2}{f} + f) - \beta\frac{xy}{f} - \gamma x)n_y$ and $g(x_0, y_0, x, y) = (x - x_0)n_x + (y - y_0)n_y$. The equation $h(x, y) = 0$ describes a hyperbola that splits the image plane in an area where $h(x, y) > 0$ and an area where $h(x, y) < 0$. The equation $g(x, y) = 0$ describes a line through the FOE, which is perpendicular to (n_x, n_y), and which separates the plane into an area where $g(x, y)$ is positive and an area where $g(x, y)$ is negative. Thus, through this inequality a region $I_{\mathbf{u_n}}$ consisting of two areas bounded by a hyperbola and a line are defined as the locations where the normal motion could take on a certain value $\mathbf{u_n}$. The two areas meet at one point, the intersection of the hyperbola and the line. This point, which contains information about the whole pattern, will be denoted by $\mathbf{S}_{\mathbf{u_n}}$ (see Fig. 11).

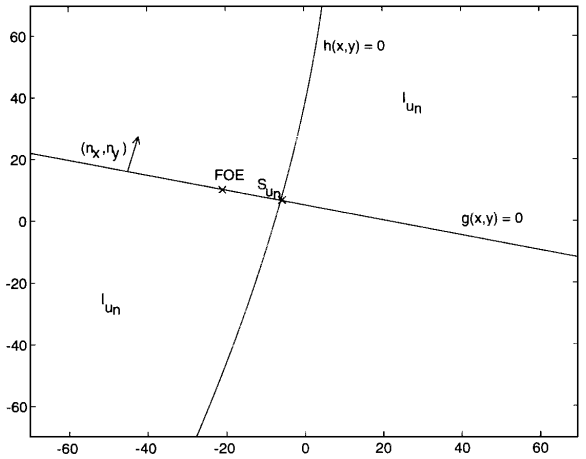

Figure 11. Iso-normal motion regions are bounded by a line ($g(x, y) = 0$) and a hyperbola ($h(x, y) = 0$).

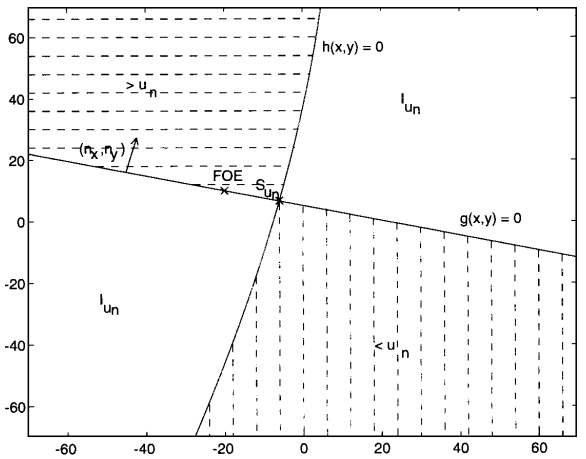

Figure 12. Separation of the image plane into areas by the values of the normal motion vectors in certain directions: In the area marked by horizontal lines all normal motion vectors in direction (n_x, n_y) are greater than u_n. In the area marked by vertical lines all normal motion vectors in direction (n_x, n_y) are smaller than u_n. Vectors of length u_n in direction (n_x, n_y) can only be in the complementary areas (the region $I_{\mathbf{u_n}}$).

In the other areas of the image plane the value of the motion vectors in direction (n_x, n_y) is constrained. Where $h(x, y) < 0$ we have $u_n > \mathbf{u}_{\text{rot}} \cdot \mathbf{n}$ (i.e., the rotational component of the normal motion is greater than u_n). Where $g(x, y) > 0$ the translational component of the normal motion is greater than zero. In the area where $h(x, y) < 0$ and $g(x, y) > 0$, we can thus conclude that the normal motion (the sum of the rotational and translational components) is greater than u_n. Similarly, where $h(x, y) > 0$ and $g(x, y) < 0$, the value of the normal motion has to be smaller than u_n (see Fig. 12).

To summarize these results, considering for a given normal motion field due to rigid motion the vectors along the gradient direction (n_x, n_y), we find that the image plane is split by a hyperbola and a line into four areas. All vectors which are of length u_n are in two opposite areas. One of the two other areas contains only values greater than u_n, and the other only values smaller than u_n.

The line $(g(x, y) = 0)$ is defined by the translational motion; it passes through the FOE and is perpendicular to the gradient (n_x, n_y) of the normal motion vector. Therefore, this line is described by only one unknown parameter (its direction is known). Furthermore, the line is independent of u_n, the value of the normal motion vector. For any general $\mathbf{u_n}$ the hyperbola $(h(u_n, x, y))$ is defined by the three rotational parameters. For the case when $u_n = 0$, the number of unknowns reduces to two ($\frac{\alpha}{\gamma}$ and $\frac{\beta}{\gamma}$ expressing the direction of the rotation axis). If we consider parallel normal motion vectors, i.e., normal motion vectors of value $k(u_n, v_n)$, where k any scalar, we find areas in the image plane which are bounded by a line that is the same for all values and hyperbolas which differ only in their linear terms (see Fig. 13).

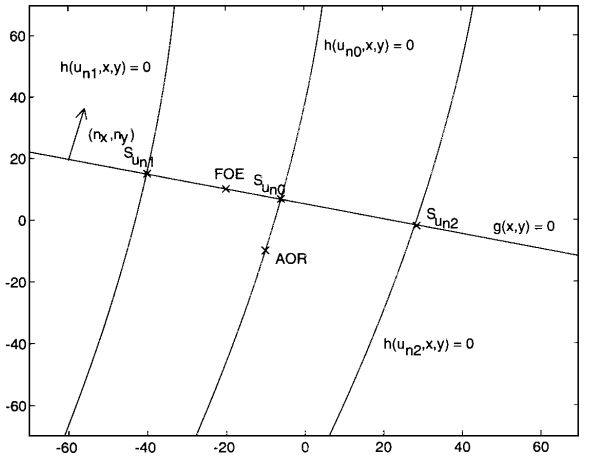

Figure 13. Iso-normal motion regions corresponding to parallel normal motion vectors: The hyperbolas $h(\mathbf{u_{n0}}, x, y)$, $h(\mathbf{u_{n1}}, x, y)$, and $h(\mathbf{u_{n2}}, x, y)$ are corresponding to the parallel normal motion vectors $\mathbf{u_{n0}}$, $\mathbf{u_{n1}}$, and $\mathbf{u_{n2}}$. The length of $\mathbf{u_{n0}}$ is zero, thus $h(\mathbf{u_{n0}}, x, y)$ passes through the AOR. The line $g(x, y) = 0$ is independent of the length of the normal motion vector and thus the same for all parallel normal motion vectors.

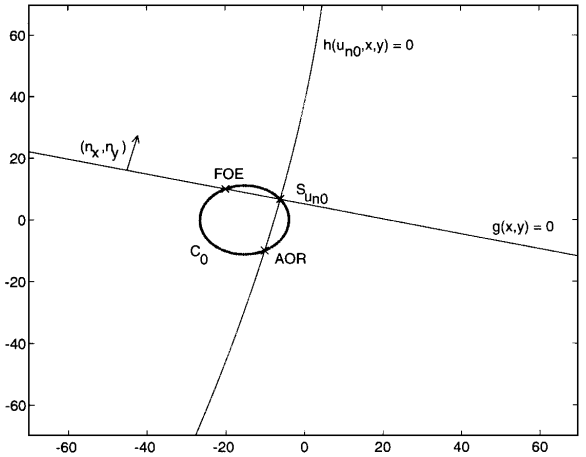

Figure 14. The intersection points $\mathbf{S_{u_n}}$ of the zero normal motion regions lie on the zero motion contour.

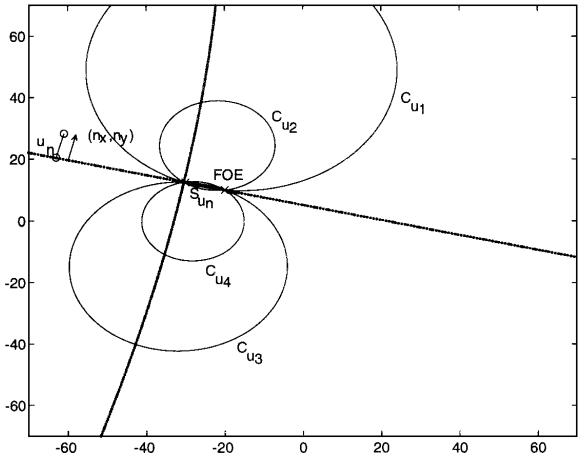

Figure 15. The iso-motion curves $C_{\mathbf{u}_1}$, $C_{\mathbf{u}_2}$, $C_{\mathbf{u}_3}$, and $C_{\mathbf{u}_4}$, (where $\mathbf{u}_1 \cdot \mathbf{n} = u_n$, $\mathbf{u}_2 \cdot \mathbf{n} = u_n$, $\mathbf{u}_3 \cdot \mathbf{n} = u_n$, $\mathbf{u}_4 \cdot \mathbf{n} = u_n$) intersect on a line through the FOE perpendicular to $\mathbf{n}$.

4.2. Relation Between Iso-Normal Motion Regions and Iso-Motion Contours

The intersection point of the line and the hyperbola $\mathbf{S_{u_n}}$ is a salient point in the description of the iso-normal motion areas. We describe here some relationships between the intersection points and the iso-motion contours. Later these relations will be exploited in the development of algorithms.

First, let us consider the zero iso-normal motion areas only. For points on the line $g(x, y) = 0$ the translational normal motion vector component in the direction of the gradient (n_x, n_y) is zero. For points along the hyperbola $h(x, y) = 0$ the rotational normal motion component in direction (n_x, n_y) is zero. Therefore, it follows that at the intersection point $\mathbf{S_{u_n}}$ the translational motion component is parallel to the rotational motion component, and thus for all zero iso-normal motion areas $\mathbf{S_{u_n}}$ lies on the zero iso-motion contour (see Fig. 14). $\mathbf{S_{u_n}}$ is also element of every $k(-n_y, n_x)$ iso-motion contour.

The following can be derived for the intersection point $\mathbf{S_{u_n}}$ of any general $\mathbf{u_n}$ iso-normal motion area: Since $\mathbf{S_{u_n}}$ lies on the line $g(x, y) = 0$, the translational motion component at $\mathbf{S_{u_n}}$ is parallel to the line and perpendicular to $\mathbf{u_n}$, and the translational normal motion component along (n_x, n_y) is always zero. Therefore, through $\mathbf{S_{u_n}}$ pass all those $\mathbf{u}$ iso motion contours for which $u_n = \mathbf{u} \cdot \mathbf{n}$ (i.e., all the motion vectors pass whose projection on the gradient direction yields in the same normal motion vector) (see Fig. 15).

4.3. Bounded Depth Measurements

The constraints developed so far are only due to rigid motion. In most practical applications upper and lower bound estimates of the distance from the image to the scene, or the scaled distance $\frac{W}{Z}$, are available. If in Eq. (13) we substitute $\tau_{\min}$ for the minimum value and $\tau_{\max}$ for the maximum value of $\frac{W}{Z}$, we obtain two equations of hyperbolas. These equations define the boundaries of the area in which normal motion vectors of a certain length and direction can be found. We will refer to these areas as normal motion bands; an illustration is given in Fig. 16.

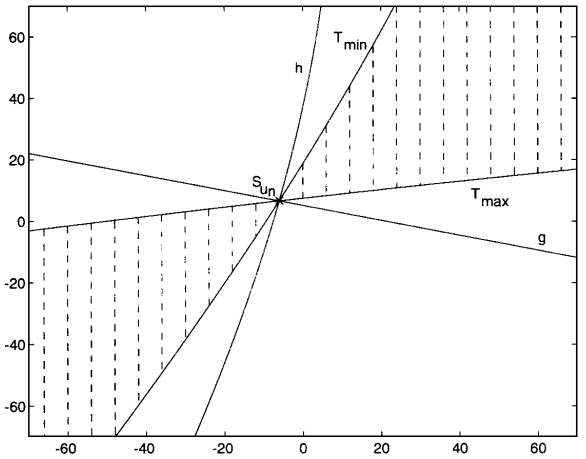

Figure 16. Bounds on the value $\frac{W}{Z}$ constrain the normal motion vectors to an area defined by two hyperbolas, the so-called normal motion band.

If the upper bound for the depth becomes infinity, the corresponding hyperbola approaches the hyperbola of the iso-normal motion area. Such situations often occur in outdoor scenes. If the lower bound for the depth becomes zero, the corresponding hyperbola approaches the line. Clearly, the smaller the possible range for the depth estimates, the smaller the bounded area. In particular, if the motion is only rotational, the measurements are only along the hyperbola of the iso-normal motion area. Considering normal motion vectors of length zero, this hyperbola passes through the AOR. If the motion is purely translational, all normal motion measurements of value zero are on the line. An illustration is given in Fig. 17. Figures 17(a), (c) and (e) show synthetically created normal motion fields. The fields in Figs. 17(c) and (e) are due to only translation and only rotation, and the normal motion field in Fig. 17(a) is due to both these motions. Overlaid over the normal motion field in 17(a) are vectors showing the gradient directions n_1 and n_2, for which normal motion vectors of length zero have been selected, and the corresponding boundaries of the normal motion areas. In this and any other implementation shown in this paper vectors of direct $\mathbf{n}$ and length u_n are selected, if they lie within an interval $[\mathbf{n} + \epsilon_{\mathbf{n}}, \mathbf{n} - \epsilon_{\mathbf{n}}]$ and $[u_n + \epsilon_{u_n}, u_n - \epsilon_{u_n}]$. In Figs.17(b), (d) and (f) the areas in the image plane, where normal motion vectors of length zero in direction n_1 and n_2 were found are marked by black and grey squares.

The following can be concluded about the intersection of general iso-normal motion bands: For different gradient directions $\mathbf{n_i}$ we consider the normal motion vectors of length u_{ni}, where u_{ni} is the projection of the same motion vector $\mathbf{u}$ (i.e., $u_{ni} = \mathbf{u} \cdot \mathbf{n_i}$). Any scaled depth value τ defines a curve as the location of normal motion vectors of value u_{ni}. For one τ the curves corresponding to different gradient directions intersect in one point. This point lies on the $\mathbf{u}$ iso-motion contour. Thus the intersection of all u_{ni} iso-normal motion bands is a curve segment that lies on the $\mathbf{u}$ iso-motion contour. In particular, all iso-normal motion areas of value zero intersect on the zero motion contour (see Fig. 18).

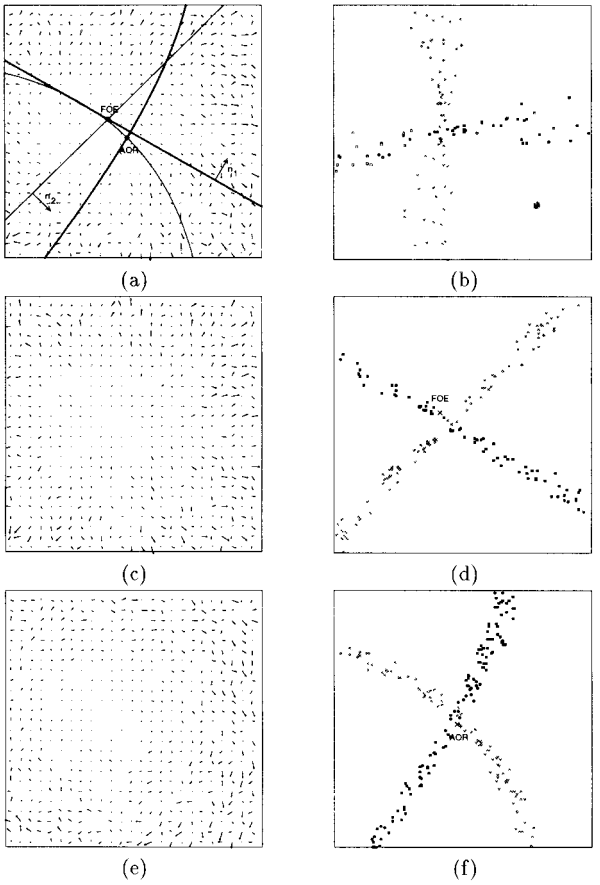

Figure 17. (a) Normal motion field due to translation and rotation. Superimposed on the vector field are the boundaries of the two normal motion areas corresponding to the vectors of length zero in direction n_1 and n_2, (b) the black and grey squares denote locations where in the normal motion field of (a) vectors of length zero in direction n_1 and n_2 were found, (c) and (d) normal motion field only due to translation and corresponding normal motion vectors of length zero in direction n_1 and n_2. The intersection of areas corresponding to different normal motion vectors of length zero gives the FOE, (e) and (f) normal motion field only due to rotation and corresponding normal motion vectors of length zero in direction n_1 and n_2. The intersection of areas corresponding to different normal motion vectors of length zero gives the AOR.

4.4. *Coaxis and Copoint Vectors*

In this section the concept of selection of normal motion vectors of a given length and direction is generalized. Instead of considering vectors of the same value, we examine various classes of vector-valued functions. In particular, we investigate the coaxis and copoint vectors, which we described in earlier work (Fermüller, 1993; Fermüller and Aloimonos, 1993).

The copoint vectors are defined with respect to a point. The (r, s) copoint vectors are defined as the normal motion vectors which are perpendicular to straight lines passing through the point (r, s). An (r, s) copoint vector at a point (x, y) is parallel to the vector $(s - y, x - r)$ (see Fig. 19).

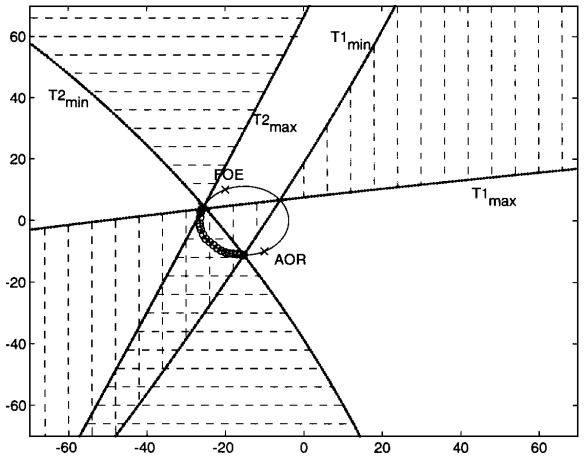

Figure 18. The normal motion bands corresponding to vectors of length zero intersect on the zero motion curve (curve segment marked by circles).

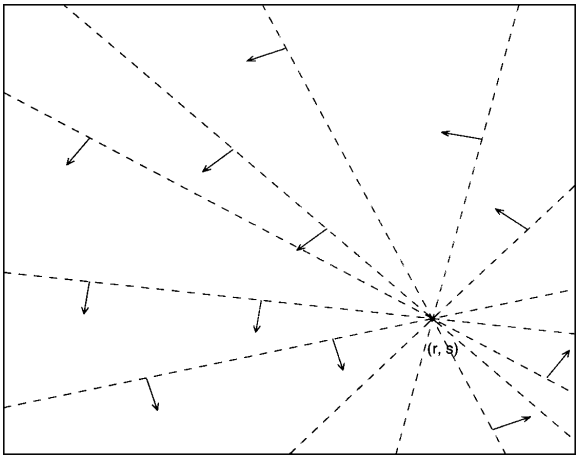

Figure 19. Copoint vectors (r, s).

The coaxis vectors are defined with respect to a direction in space. The (A, B, C) coaxis vectors are defined as follows: A line through the image formation center defined by the directional cosines (A, B, C) defines a family of cones with axis (A, B, C) and apex at the origin. The intersection of these cones with the image plane gives rise to conic sections. The normal motion vectors perpendicular to these conic sections are called (A, B, C) coaxis vectors. At every point (x, y) a coaxis vector is parallel to the vector $(-A(y^2 + f^2) + Bxy + Cx,\ Axy - B(x^2 + f^2) + Cy)$ (see Fig. 20).

As in the case of the iso-normal motion vectors, we choose vectors of a given length and direction and evaluate the regions with positive depth measurements. We

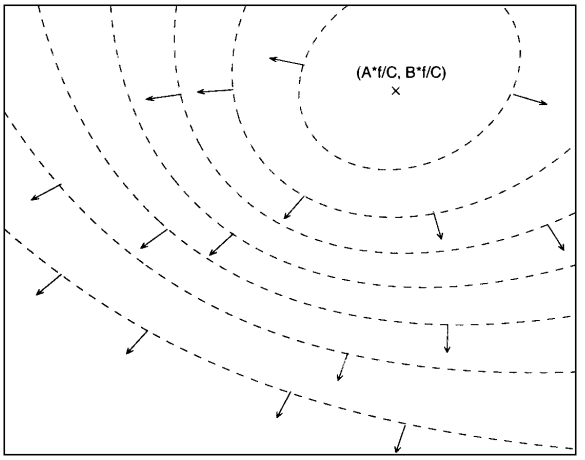

Figure 20. (A, B, C) coaxis vectors.

consider the (r, s) copoint vectors and the (A, B, C) coaxis vectors of length $u_n(x, y)$ (with $u_n(x, y)$ a function in x and y). Where $\frac{W}{Z} > 0$ the following inequalities hold:

$$
\begin{aligned}
&[y(x_0 - r) - x(y_0 - s) - x_0 s + y_0 r] \\
&\quad \cdot \left[u_n(x, y) - \frac{x^2}{f}(\beta s + \gamma f) - \frac{y^2}{f}(\alpha r + \gamma f) \right. \\
&\qquad + xy\left(\frac{\alpha s}{f} + \frac{\beta r}{f}\right) + y(\gamma s + \beta f) \\
&\qquad \left. + x(\gamma r + \alpha f) - (\alpha f r + \beta f s) \right] > 0 \qquad (15) \\
&\left[u_n(x, y) - \left(y\left(\frac{C\alpha}{f} - \frac{A\gamma}{f}\right) \right. \right. \\
&\qquad \left. \left. + x\left(\frac{B\gamma}{f} - \frac{C\beta}{f}\right) + A\beta - B\alpha \right)(x^2 + y^2 + f^2) \right] \\
&\quad \cdot \left[y^2\left(\frac{Ax_0}{f} + C\right) - xy\left(\frac{Bx_0}{f} + \frac{Ay_0}{f}\right) \right. \\
&\qquad + x^2\left(\frac{By_0}{f} + C\right) - y(Bf + Cy_0) \\
&\qquad \left. - x(Af + Cx_0) + Ax_0 f + By_0 f \right] > 0 \qquad (16)
\end{aligned}
$$

For $u_n(x, y) = 0$ we obtain regions defined by a line and a conic section. In the case of the copoint vectors the line separates the translational components and the conic separates the rotational components of the vectors. The line passes through the FOE and also through the point (r, s), and thus it can be described by only one unknown. The conic is specified by only two unknowns, $\frac{\alpha f}{\gamma}$ and $\frac{\beta f}{\gamma}$. In the case of the coaxis vectors,

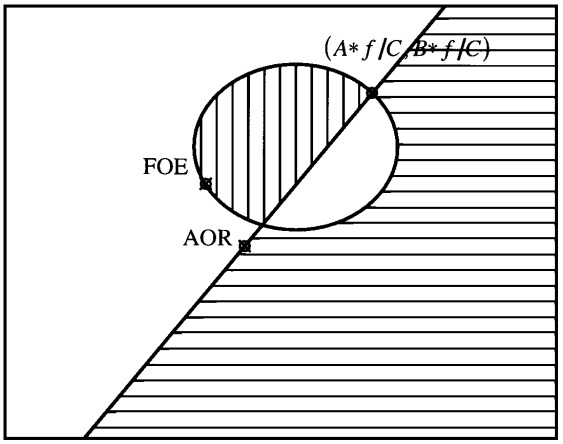

Figure 21. Separation of (A, B, C) coaxis vectors whose directions are shown in Fig. 20: A line passing through the AOR separates the positive and negative rotational components. A conic through the FOE separates the positive and negative translational components. In the area marked by horizontal lines all (A, B, C) coaxis vectors are greater than zero. In the area marked by vertical lines all (A, B, C) coaxis vectors are smaller than zero. The two other areas contain all the (A, B, C) coaxis vectors of length zero.

the line separates the rotational components. It passes through the AOR and through the point (r, s) and thus it is also described by only one unknown. The conic separates the translational components. It is defined by the two coordinates of the FOE, (x_0, y_0). The intersection of the lines and the conics lies on the zero motion curve. One of the two other regions defined by the above described curves contains only vectors of length greater than zero, and the other contains only vectors smaller than zero. An illustration is given in Fig. 21, which shows these regions for the class of coaxis vectors displayed on Fig. 20.

It becomes clear that the normal motion vectors of same length and direction can be considered as special cases of the copoint vectors. They represent the copoint vectors, for which r and s both are ∞ and $\frac{r}{s} = \frac{-n_y}{n_x}$. A special class of coaxis vectors, those which correspond to an axis parallel to the XY-plane, is very similar to the iso-normal motion vectors. For all classes of coaxis vectors $(A, B, 0)$ the slope of the line separating the rotational components is $\frac{A}{B}$ and the conics are all hyperbolas.

5. Applications

The constraints developed in this paper allow us to make explicit aspects of the structure of motion fields and normal motion fields which are due to rigid motion. These constraints can be exploited in a variety of algorithms dealing with visual navigation tasks. In particular, they could be used to verify the rigidity of a given motion field in order to detect and localize independent motion; to estimate the 3D rigid motion or provide bounds for the motion parameters that in conjunction with other algorithms could lead to accurate estimation; and to address problems in visuomotor control in robotic applications such as servoing or stabilization. In the remainder of this section we will describe in more detail ideas that could be used in algorithmic procedures for 3D motion estimation.

5.1. *Using Motion Vectors*

Knowledge of any single iso-motion contour is sufficient to derive the 3D motion. Thus the localization of any such contour provides the motion parameters. Iso-motion contours could be localized with simple matching techniques using filters which are tuned to respond to image points in different frames being a certain distance apart (see Fig. 22). Finding motion vectors of a certain length and direction by means of predefined filters is a decision problem and thus easier and of lower complexity than computing a motion field.

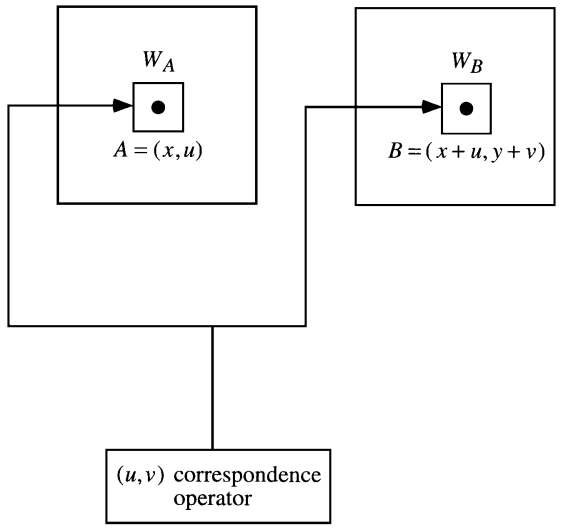

Figure 22. To test whether points $A = (x, y)$ and $B = (x+u, y+v)$ correspond, we test how well two windows w_A and w_B placed around the point A and B match. With a set of correspondence operators tuned to different values (u, v) the points on the (u, v) iso-motion contours are located.

In addition, the various relationships between iso-motion contours described in Section 3 can be used to increase the accuracy of the computation of iso-motion contours. We can describe every point as the intersection of a certain class of iso-motion contours: the FOE is the intersection of all iso-motion contours; different $k\mathbf{u}$ iso-motion contours intersect at a point on the zero motion contour; and any point on a general $\mathbf{C_u}$ iso-motion contour can be considered as the intersection of a family of iso-motion contours as described in Eq. (7).

Furthermore, knowledge about the directions of the motion vectors along iso-motion contours can be of use in the verification of the contours' correct locations. As described in Section 3.2, for every point along any $\mathbf{u}$ iso-motion contour the following holds: If we subtract $\mathbf{u}$ from the motion vector $\mathbf{v}$ at $\mathbf{P}$, we obtain a vector $\mathbf{v}_-$, which is parallel to the translational motion component of $\mathbf{v}$. In particular, for every point along the zero motion contour the motion vector is in the direction of the translational motion component. The preceding discussion demonstrates that even if there is no iso-motion contour available, but we have at our disposal a set of points (at least two) with their associated motion vectors, and we know on which iso-motion contour each point lies, the position of the FOE is uniquely determined (as shown in Figs. 6 and 7).

5.2. Using Normal Motion Vectors

Similarly, the iso-normal motion areas as well as the regions containing coaxis and copoint vectors of a certain length and direction can be used in the recovery of the 3D motion. The normal motion regions can be obtained by localizing their boundaries. In particular, the normal motion vectors of length zero are bounded by curves which can be described by only three parameters. Thus a simple search technique in a three-dimensional space, such as in Fermüller (1993), Fermüller and Aloimonos (1993), could be employed to find the 3D motion parameters.

The iso-normal motion areas, however, also allow to obtain bounds on the solutions for the motion parameters in very simple ways. Computations of this kind might be used in combination with other techniques, such as the search techniques described above, for example as preprocessing modules to reduce the amount of search.

A possible area for the FOE can be obtained by using iso-normal motion vectors in different directions. The normal motion vectors of a given value are located within the normal motion bands (see Fig. 16). The normal motion bands consist of two areas meeting at the point $\mathbf{S_{u_n}}$. Through $\mathbf{S_{u_n}}$ and the FOE passes the boundary line of the iso-normal motion areas, which also separates the translational motion components (Fig. 11). The slope of the line is known; it is perpendicular to the direction of the normal motion. The exact position of the line is defined by the location where the normal motion band is thinnest. It may not be possible to locate one point and thus the exact line, but only a bounded area which contains the line. Since all iso-normal motion areas of different lengths but the same direction define the same line, this bounded area can be located by means of a number of iso-normal motion bands corresponding to parallel motion vectors. The intersection of at least two such bounded areas corresponding to normal motion vectors in different directions gives an area in which the FOE lies. This is demonstrated in Fig. 24. Figure 23 shows the synthetic normal flow field, which was used as input data for the localization of the translation and rotation axis demonstrated in the following three figures. (Figs. 24, 25, 26). The image size is 300×300, the focal length is 100 pixel, the origin is at the center of the image. The translation was $(-0.1, 0.1, 0.5)$ and the rotation was $(0.005 - 0.002, 0.01)$, where the depth was chosen randomly in an interval between 20.0 and 70.0.

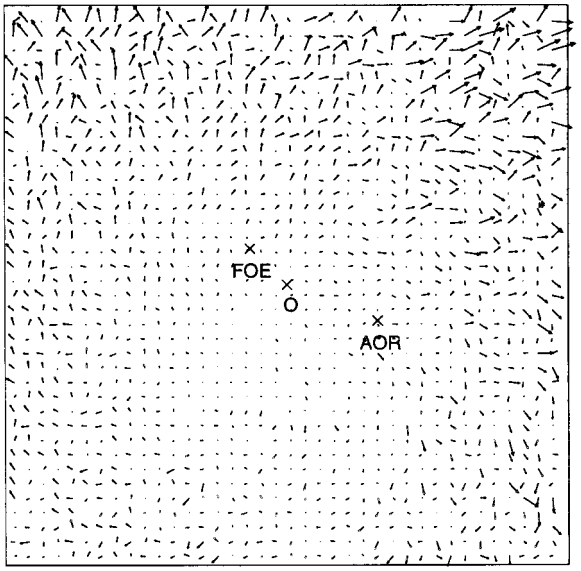

Figure 23. Synthetic normal motion field used as input data for the localization of the FOE and AOR shown in the next three figures.

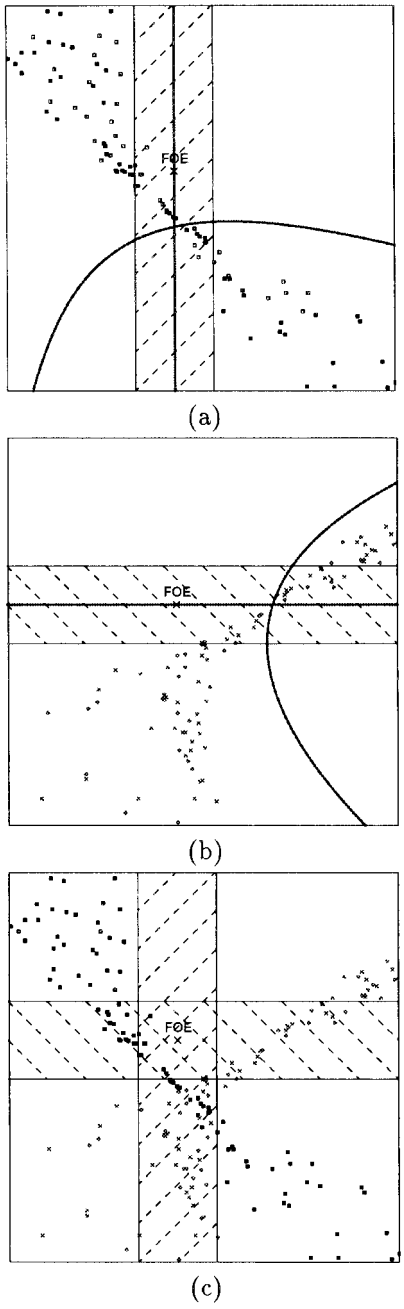

Figure 24. Localization of FOE: (a) Normal motion band due to normal motion vectors of a certain length parallel to the x-axis and corresponding curves $g(x, y)$ and $h(x, y)$ defining the normal motion area. By localizing, where this normal motion band is thinnest a bounded area for the line separating the translational normal motion components is found (marked by diagonal lines). (b) Normal motion band due to normal motion vectors of a certain length parallel to the y-axis with overlaid curves $g(x, y)$ and $h(x, y)$ defining the normal motion area and localization of bounded area for the line separating the translational normal motion components (marked by diagonal lines). (c) The intersection of these areas gives a bounded area for the FOE.

Instead of focusing on the thinnest location of the normal motion bands, one could consider various normal motion bands corresponding to different lengths but the same direction. Two such iso-normal motion areas cannot intersect in an area that contains the line. Thus an area for the line passing through the FOE can be located as the region between regions where iso-normal motion areas intersect (see Fig. 25).

Just as a line passing through the FOE bounds the iso-normal motion regions, a line passing through the point where the rotation axis pierces the image plane (AOR) bounds regions separating the $(A, B, 0)$ coaxis vectors of length zero. By finding the locations where the areas separating the $(A, B, 0)$ coaxis patterns are thinnest and intersecting different such areas, a bounded region for the AOR can be located (see Fig. 26).

In general one cannot solely rely on single bands of normal motion vectors to locate bounding areas for the FOE and AOR, simply because the structure of the bands also depends on the distribution of the image gradients. If in a certain area there are no gradients available in a desired direction, the appropriate band will not exist there (or be thin). On the other hand, a complete search in subspaces of the rigid motion parameters for the boundaries of the iso-normal motion regions (or the areas with normal flow values greater u_n and smaller u_n, or areas defined by the coaxis vectors) will always lead to correct solutions. The essential information about the location of the regions' boundaries lies in the location of the iso-normal vectors. Thus a complete search will not be necessary and ideal strategies will be combination algorithms that can make efficient use of the relevant information without missing solutions.

The following experiments give a demonstration of the localization of bounded areas for the FOE and AOR using two of the algorithms described above for a calibrated motion sequence.

Figure 27(a) shows the first image of the sequence and Fig. 27(b) shows the normal motion field computed between the first and the second frame. The image size is 574×652, the FOE is at $(x, y) = (197, 136)$ and the AOR is at $(x, y) = (413, 124)$ (with the origin of the coordinate system at the left upper corner). In Fig. 28(a) the points with iso-normal motion vectors parallel to the y-axis of three different lengths (0.3, 0.1, and -0.1 pixels) are displayed in red green and blue. These normal motion vectors constrain the FOE to lie in an area bounded by the two horizontal lines where there is no intersection of the differently colored iso-motion areas, in between the regions of intersection. Similarly, the normal motion vectors parallel to the

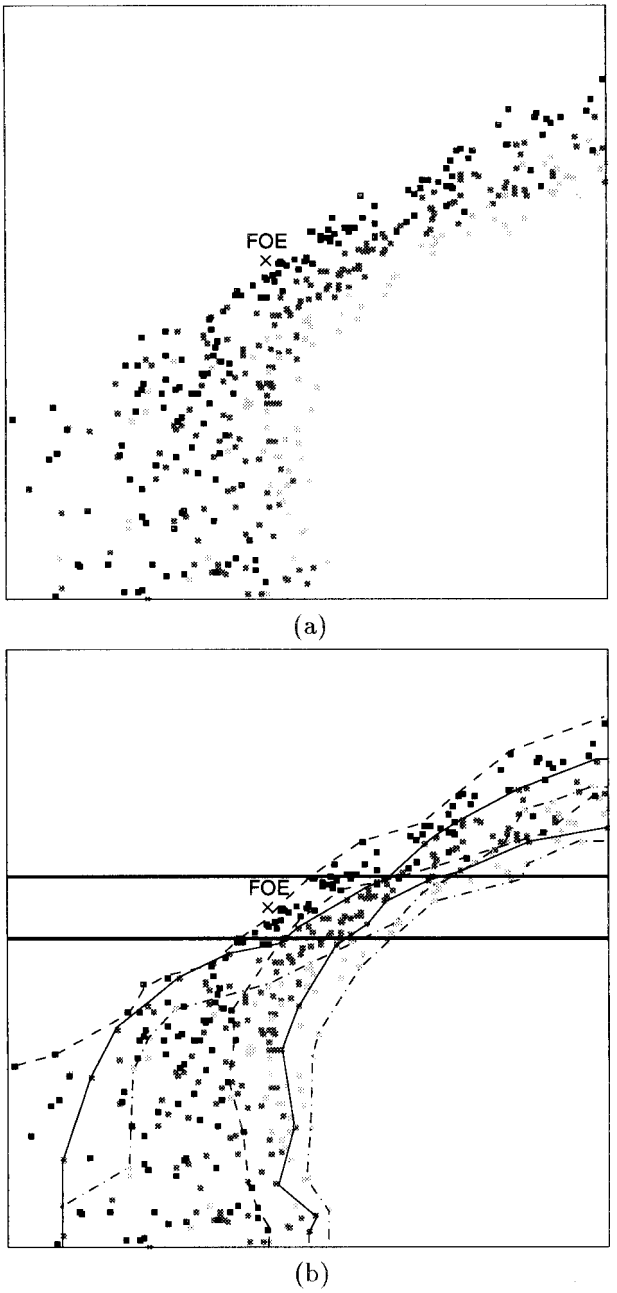

Figure 25. Localization of FOE: The FOE cannot lie within the areas where the normal motion bands corresponding to parallel normal motion vectors intersect. (a) Normal motion vectors parallel to the y-axis of three different lengths (displayed in dark, medium, and light grey). (b) Polygonal approximation of the boundaries of normal motion bands and localization of an area in which the FOE can lie.

x-axis (of length -0.3, 0.0 and 0.3) constrain the FOE to lie in an area bounded by two vertical lines as shown in Fig. 28(b). The intersection of the areas found in Figs. 28(a) and (b) gives a bounded area for the FOE (see Fig. 28(c)).

Figure 29 shows the results of the algorithm using $(A, B, 0)$ coaxis vectors of length zero to locate the AOR by finding the locations where the bands are thinnest. Figures 29(a)–(d) show the results for the the (1, 0, 0) coaxis vectors, (0, 1, 0) coaxis vectors, and

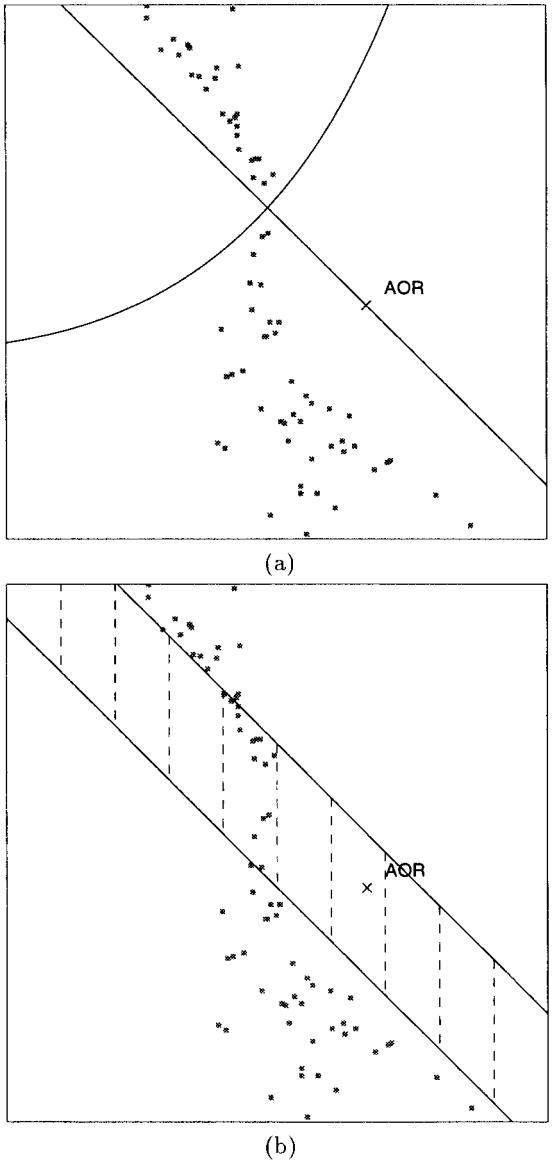

Figure 26. Localization of the AOR with $(A, B, 0)$ coaxis vectors: (a) $(0.707, -0.707, 0)$ coaxis vectors of length zero and curves separating the positive from the negative translational and rotational normal motion components. (b) Localization of a bounded area in which the AOR lies.

(0.707, 0.707, 0) coaxis vectors and their intersection in red, green and blue.

5.3. Combined Use of Motion and Normal Motion

Of course, the iso-motion and iso-normal motion constraints can also be used in a combined manner. To locate iso-motion contours normal motion vectors can be employed. For example, the intersection of normal motion bands (belonging to normal motion vectors originating from one motion vector) gives a segment of the corresponding iso-motion contour (see Figs. 14 and 15).

6. Conclusions

The motion field or the displacement field due to rigid motion on a system's retina possesses a global structure that is independent of the scene in view and depends only on the parameters of the underlying 3D motion. In this paper we studied this structure by analyzing the geometry of the iso-motion contours and iso-motion regions, i.e., the loci on the retina where the motion vector (or the normal motion vector) could obtain a certain value. We found that the iso-motion curves and the boundaries of the iso-normal motion areas are of second order and their form depends on the 3D motion parameters. The theory described here can find several applications in problems of visual motion interpretation as well as calibration, or in general, in problems related to the matching of two views and its interpretation (Fernmüller and Aloimonos, 1996).

Appendix A

Iso-Motion Contours and Iso-Normal Motion Area for Spherical Projection

Today's commercially available electronic cameras used in robotic systems and utilized in our experiments have image surfaces that are best approximated by a plane. For this reason the analysis in this paper was performed for a planar retina as well. However, from a geometric point of view, for the purpose of analyzing visual motion globally, the use of a spherical retina is much more natural. This is because it provides us with a 360° field of view. On the sphere the iso-motion contours and the iso-normal motion areas take a simple form. Their derivation from first principles provides valuable geometric intuition into the problem and is described here.

On a sphere of radius f (see Fig. 30), the image $\mathbf{r}$ of every point $\mathbf{R}$ is

$$\mathbf{r} = \frac{\mathbf{R}\, f}{|\mathbf{R}|}$$

with $|\mathbf{R}|$ being the norm of the vector $\mathbf{R}$; Recalling from Eq. (1), if we project the 3D-motion on the sphere the

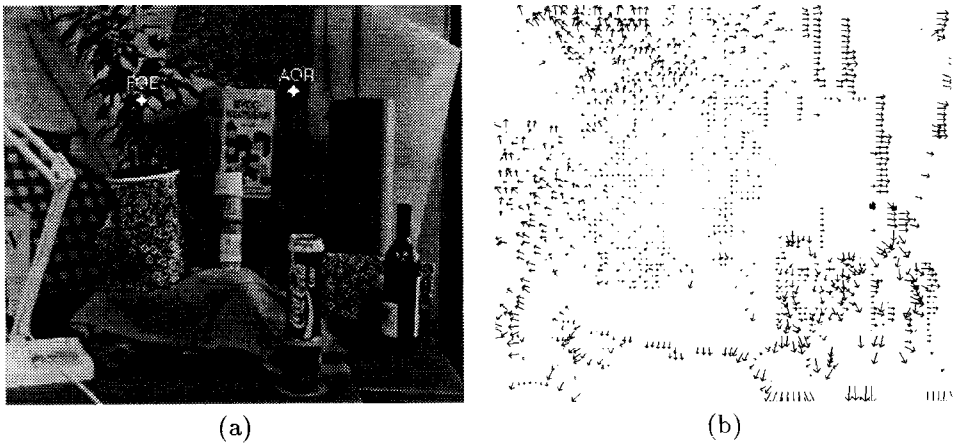

(a) (b)

Figure 27. (a) First frame of a motion sequence. (b) Normal motion field.

motion vector $\dot{\mathbf{r}}$ can be expressed as

$$\dot{\mathbf{r}} = \frac{1}{|\mathbf{R}|}\left(\frac{1}{f}(\mathbf{t}\cdot\mathbf{r})\mathbf{r} - f\,\mathbf{t}\right) - \boldsymbol{\omega}\times\mathbf{r}. \qquad \text{(A1)}$$

When employing general imaging surfaces, the motion vectors at a surface point are defined on the local tangent plane. In the discussion of $\mathbf{u}$ iso-motion contours on the plane, we used a simplified notation and did not mention that the vector $\mathbf{u}$ actually results from the projection of a 3D vector on the local tangent plane which happens to be the same everywhere. However, for the case of a spherical retina we have to be more general and provide definitions in the form of projections of 3D vectors on the local tangent plane. In the following we use the negative value of the projection of a vector. Thus, for example, if $\mathbf{u}$ is a 3D vector, the $\mathbf{u}$ iso-motion contours on a sphere with radius one ($f = 1$), are defined as the locus of points $\mathbf{r}$ on the sphere where the motion vector has the value $(\mathbf{u}\cdot\mathbf{r})\mathbf{r}-\mathbf{u}$. The following four propositions characterize the structure and form of the iso-motion contours (Propositions 1–3) and iso-normal motion areas (Proposition 4) on the unit sphere:

Proposition 1. *For a rigid motion field on the sphere the geometrical locus of points at which the motion vector could have the value* $(\mathbf{u}\cdot\mathbf{r})\mathbf{r}-\mathbf{u}$ *is described by a second order equation that in general gives rise to one or two curves. These curve*(*s*) *pass through the FOE and the FOC* (*the points where* $\mathbf{t}$ *pierces the sphere*) *and the points* $\mathbf{R}_{\mathbf{u}}$ ($\mathbf{R}_{\mathbf{u}_1}$ *and* $\mathbf{R}_{\mathbf{u}_2}$) (*where the rotational component of the motion is equal to* $(\mathbf{u}\cdot\mathbf{r})\mathbf{r}-\mathbf{u}$).

Proof: For the locus of points $\mathbf{r}$ with motion vector $(\mathbf{u}\cdot\mathbf{r})\mathbf{r}-\mathbf{u}$ using (A1) we obtain

$$\frac{1}{|\mathbf{R}|}((\mathbf{t}\cdot\mathbf{r})\mathbf{r}-\mathbf{t}) - (\boldsymbol{\omega}\times\mathbf{r}) = (\mathbf{u}\cdot\mathbf{r})\mathbf{r}-\mathbf{u}. \qquad \text{(A2)}$$

If $\mathbf{u} = 0$ we obtain

$$\begin{aligned} &((\mathbf{t}\cdot\mathbf{r})\mathbf{r}-\mathbf{t})\times(\boldsymbol{\omega}\times\mathbf{r}) = 0 \\ \text{or}\quad &-(\mathbf{t}\cdot\mathbf{r})(\mathbf{r}\cdot\boldsymbol{\omega})\mathbf{r} + (\mathbf{t}\cdot\boldsymbol{\omega})\mathbf{r} = 0 \\ \text{and thus}\quad &\mathbf{t}\cdot\boldsymbol{\omega} - (\mathbf{t}\cdot\mathbf{r})(\mathbf{r}\cdot\boldsymbol{\omega}) = 0. \end{aligned} \qquad \text{(A3)}$$

Otherwise, projecting both sides of (A2) on the vector $((\boldsymbol{\omega}\cdot\mathbf{r})\mathbf{r}-\boldsymbol{\omega})$, provided that $\boldsymbol{\omega}\times\mathbf{r}\neq 0$ and on the vector $\mathbf{u}\times\mathbf{r}$, provided that $\mathbf{u}\times\mathbf{r}\neq 0$ gives:

$$\begin{aligned} &\frac{1}{|\mathbf{R}|}(\mathbf{t}\cdot\boldsymbol{\omega} - (\mathbf{t}\cdot\mathbf{r})(\mathbf{r}\cdot\boldsymbol{\omega})) \\ &\quad = \mathbf{u}\cdot\boldsymbol{\omega} - (\mathbf{u}\cdot\mathbf{r})(\boldsymbol{\omega}\cdot\mathbf{r}) \end{aligned} \qquad \text{(A4)}$$

and

$$-\frac{1}{|\mathbf{R}|}\mathbf{t}\cdot(\mathbf{u}\times\mathbf{r}) = \mathbf{u}\cdot\boldsymbol{\omega} - (\mathbf{u}\cdot\mathbf{r})(\boldsymbol{\omega}\cdot\mathbf{r}) \qquad \text{(A5)}$$

Equating the left-hand side of Eq. (A4) with the left-hand side of Eq. (A5) we derive

$$(\mathbf{r}\cdot\boldsymbol{\omega})(\mathbf{r}\cdot\mathbf{t}) - (\mathbf{t}\cdot\boldsymbol{\omega}) + (\mathbf{u}\times\mathbf{t})\cdot\mathbf{r} = 0 \qquad \text{(A6)}$$

Each of the Eqs. (A3) and (A6) describes a second order curve on the sphere and gives the locus of points, where the motion vector could take the value $(\mathbf{u}\cdot\mathbf{r})\mathbf{r}-\mathbf{u}$.

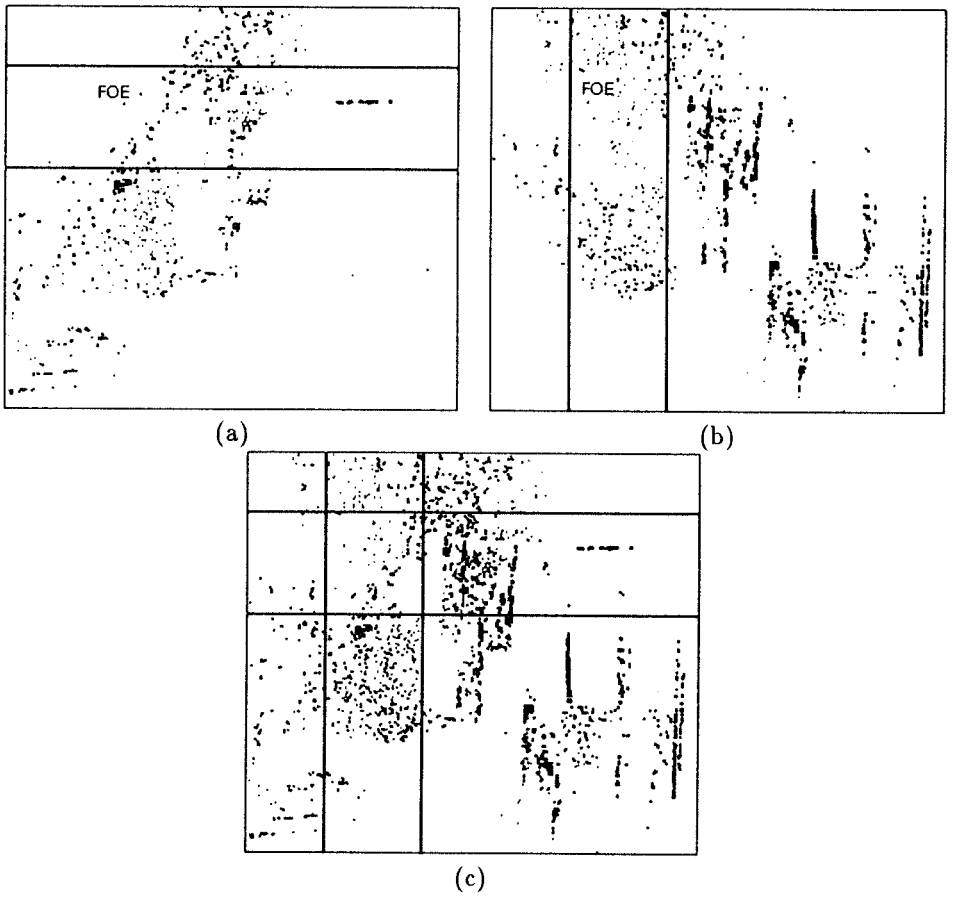

Figure 28. Localization of the FOE from normal flow vectors of same direction and different length. (a) Normal motion vectors parallel to the y-axis of three different lengths constrain the FOE to lie in an area in between the two horizontal lines. The corresponding image points are shown in red, green, and blue. (b) normal motion vectors parallel to the x-axis of three different lengths constrain the FOE to lie in the area in between the two vertical lines. (c) the intersection of the areas found in (a) and (b) provides a bounded area for the location of the FOE.

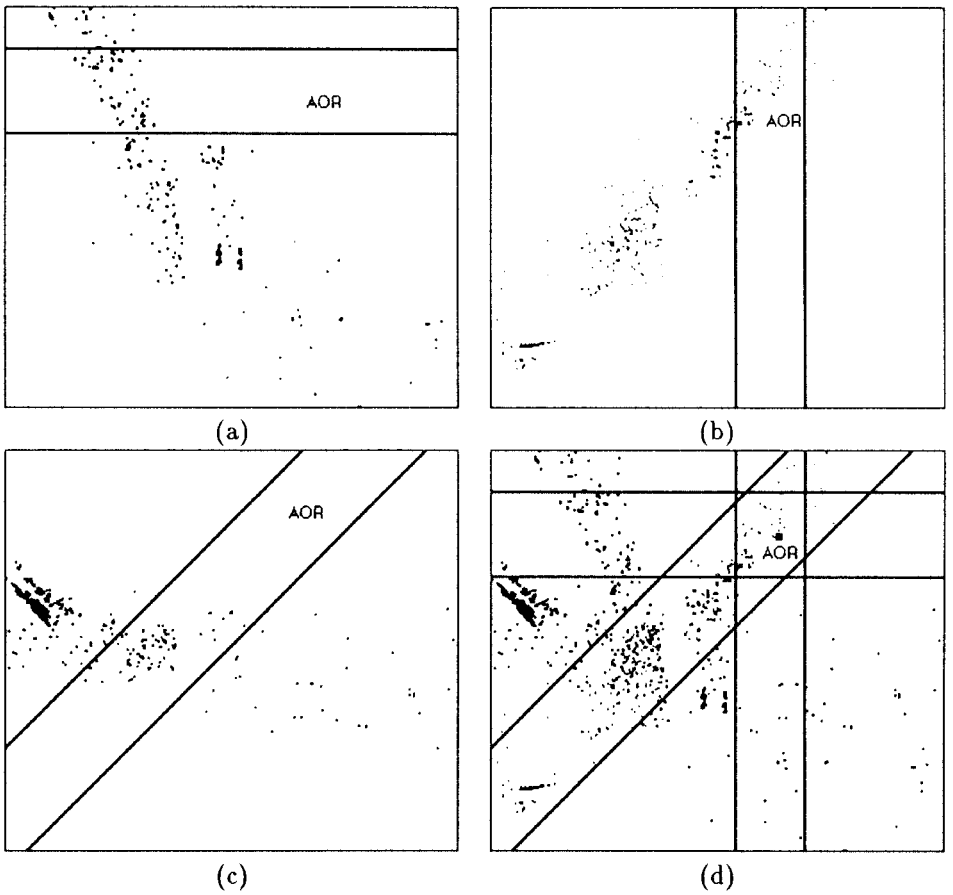

Figure 29. Localization of the AOR from normal flow vectors of $(A, B, 0)$ coaxis vectors of length zero through the location of areas where bands are thinnest, (a) $(1, 0, 0)$ coaxis vectors (red), (b) $(0, 1, 0)$ coaxis vectors (green), (c) $(0.707, 0.707, 0)$ coaxis vectors (blue), (d) the intersection of the areas found in (a), (b), and (c) provides a bounded area for the location of the AOR.

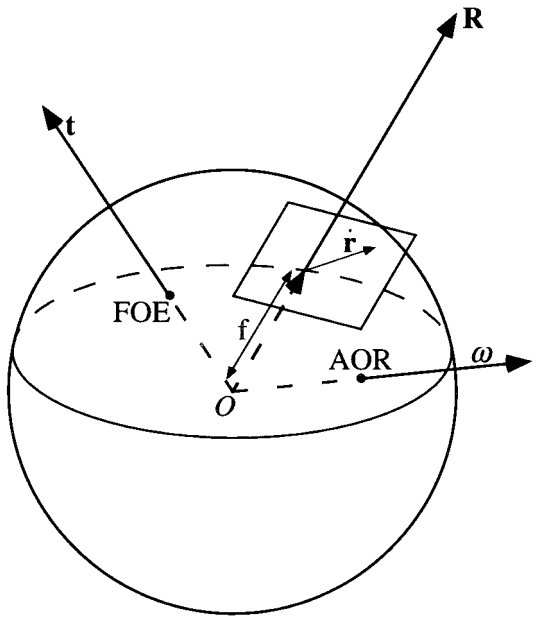

Figure 30. Image formation using perspective projection on a spherical retina.

To show that the points $\mathbf{R_u}$ lie on the curve(s) described by (A6) let us denote by $\mathbf{r_1}$ the vector $O\vec{\mathbf{R}}_u$. Then

$$-\boldsymbol{\omega} \times \mathbf{r_1} = (\mathbf{u} \cdot \mathbf{r_1})\mathbf{r_1} - \mathbf{u}. \tag{A7}$$

From (A6) we obtain the following constraint for the points $\mathbf{r_1}$:

$$(\mathbf{t} \times (\boldsymbol{\omega} \times \mathbf{r_1})) \cdot \mathbf{r_1} + (\mathbf{u} \times \mathbf{t}) \cdot \mathbf{r_1} = 0 \tag{A8}$$

Substituting in (A8) for $\boldsymbol{\omega} \times \mathbf{r_1}$ from (A7), it can be verified that $\mathbf{r_1}$ is a point on the curves. □

As can be seen from Eqs. (A3) and (A6), for the case when $\mathbf{u} = 0$ or when $\mathbf{u} \times \mathbf{t} = 0$ (i.e., $\mathbf{u}$ is parallel to $\mathbf{t}$) we always have two curves which pass through the FOE and the AOR.

Figures 31 and 32 show iso-motion curves for different values of $\mathbf{t}$, $\boldsymbol{\omega}$ and $\mathbf{u}$. In Fig. 31 four zero iso-motion contours (C_1 to C_4) are displayed, which are defined by the same $\mathbf{t}$ and different vectors ω, where the angle α between $\mathbf{t}$ and $\boldsymbol{\omega}$ increases from C_1 to C_4. For $\alpha < 90^\circ$ one of the curves contains $\mathbf{t}_0$ and $\boldsymbol{\omega}_0$ (where $\mathbf{t}_0$ and $\boldsymbol{\omega}_0$ are the unit vectors corresponding to $\mathbf{t}$ and $\boldsymbol{\omega}$), and the other contains $-\mathbf{t}_0$ and $-\boldsymbol{\omega}_0$ (C_1 and C_2 in Figs. 31(a) and (b)). For the case when $\alpha = 90$ the curves become two great circles; one orthogonal to $\mathbf{t}$, the other orthogonal to $\boldsymbol{\omega}$ (C_3 in Fig. 31(c)). This can also be seen from Eq. (A3), $\mathbf{t} \cdot \boldsymbol{\omega}$ becomes 0, and thus $\mathbf{r}$ has to perpendicular to either $\mathbf{t}$ or $\boldsymbol{\omega}$. When $\alpha > 90^\circ$ one of the curves passes through $\mathbf{t}_0$ and $-\boldsymbol{\omega}_0$ and the other through $-\mathbf{t}_0$ and $\boldsymbol{\omega}_0$ (C_4 in Fig. 31(d)).

Figure 32 shows iso-motion contours defined by the same $\mathbf{t}$ and $\boldsymbol{\omega}$ and parallel vectors $\mathbf{u}$. As one can see from Eqs. (A6) and (A3), if $\mathbf{u} \neq 0$ additional linear terms are introduced, and the locus becomes either one or two curves. As the length of $\mathbf{u}$ becomes large with regard to $\boldsymbol{\omega}$ and $\mathbf{t}$, the curve converges to the great circle ($(\mathbf{t} \times \mathbf{u}) \cdot \mathbf{r} = 0$).

Next we consider iso-motion curves corresponding to parallel vectors. We give a characterization of such families of iso-motion contours by showing first where on the sphere the points $\mathbf{R_u}$ lie, and second where these iso-motion contours intersect.

Proposition 2. *For a family of $k\mathbf{u}$ iso-motion contours, where $k \in \Re$ and $\mathbf{u}$ is a vector of unit length, the points $\mathbf{R}_{k\mathbf{u}}$ (the points on each $k\mathbf{u}$ iso-motion contour for which the rotational motion component is equal to $k((\mathbf{u} \cdot \mathbf{r})\mathbf{r} - \mathbf{u})$) lie on second order curves that contain the points $\mathbf{u}$, $-\mathbf{u}$, $\boldsymbol{\omega}$ and $-\boldsymbol{\omega}$ (see* Fig. 33).

Proof: $\mathbf{r}$ at the points $\mathbf{R_u}$ on the $k\mathbf{u}$ iso-motion contours has to satisfy

$$k((\mathbf{u} \cdot \mathbf{r})\mathbf{r} - \mathbf{u}) = -\boldsymbol{\omega} \times \mathbf{r} \tag{A9}$$

Thus, it follows that

$$((\mathbf{u} \cdot \mathbf{r})\mathbf{r} - \mathbf{u}) \times (\boldsymbol{\omega} \times \mathbf{r}) = 0$$

or

$$\mathbf{u} \cdot \boldsymbol{\omega} - (\mathbf{u} \cdot \mathbf{r})(\boldsymbol{\omega} \cdot \mathbf{r}) = 0. \tag{A10}$$

Equation (A10) describes a second order equation, which always gives two curves passing through $\mathbf{u}$, $-\mathbf{u}$, $\boldsymbol{\omega}$, and $-\boldsymbol{\omega}$. □

Proposition 3. *All $k\mathbf{u}$ iso-motion contours, where $k \in \Re$ and $\mathbf{u}$ is a motion vector of unit length, intersect in the same points, which lie in a plane. For the general case, if $(\mathbf{u} \times \mathbf{t}) \cdot (\mathbf{t} \times \boldsymbol{\omega}) \neq 0$ these are four points. Two of them are the FOE and the FOC. The two other points denoted as $\mathbf{P}_{k\mathbf{u}}$ and $-\mathbf{P}_{k\mathbf{u}}$ have coordinates $\frac{\mathbf{t}+\lambda\mathbf{u}}{||\mathbf{t}+\lambda\mathbf{u}||}$ and $-\frac{\mathbf{t}+\lambda\mathbf{u}}{||\mathbf{t}+\lambda\mathbf{u}||}$ with $\lambda = \frac{(\mathbf{u}\cdot\boldsymbol{\omega})\mathbf{t}^2 - (\mathbf{t}\cdot\mathbf{u})(\mathbf{t}\cdot\boldsymbol{\omega})}{\mathbf{t}\cdot\boldsymbol{\omega} - (\mathbf{t}\cdot\mathbf{u})(\mathbf{u}\cdot\boldsymbol{\omega})}$ (Fig.* 34).

Proof: Let us intersect two elements of the family of $k\mathbf{u}$ iso-motion contours. Considering Eq. (A6) which

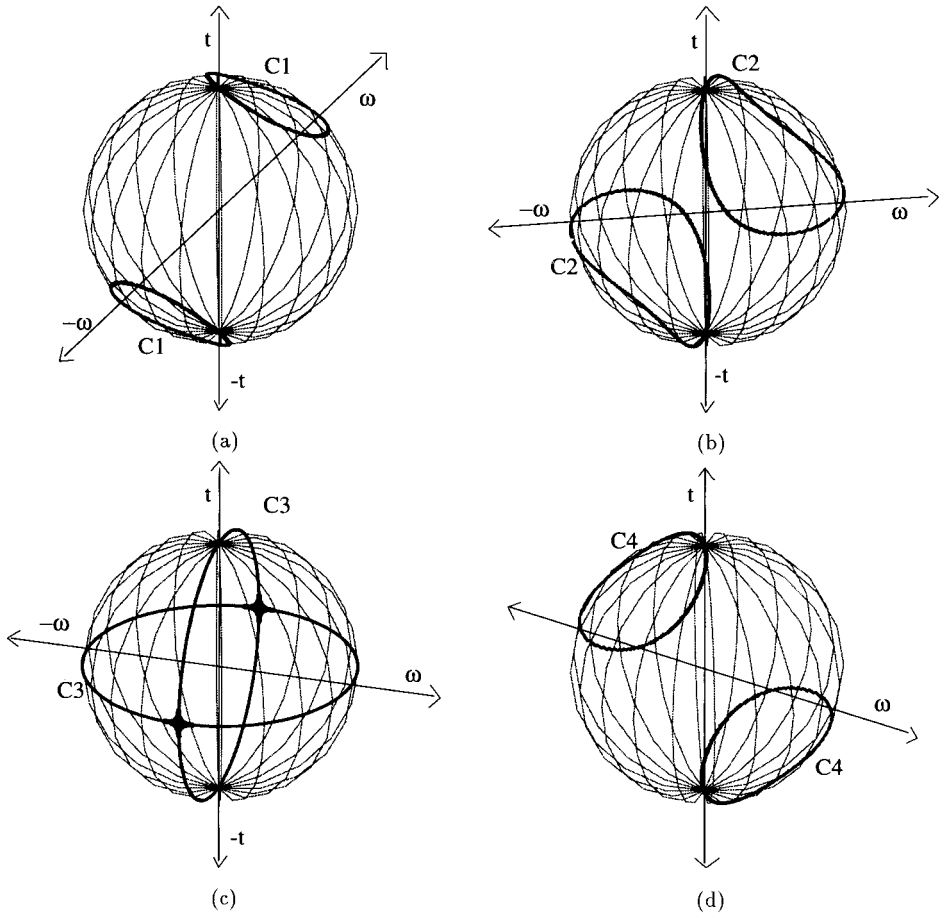

Figure 31. The locus of points on the sphere for which the motion vector could have the value $(\mathbf{u} \cdot \mathbf{r})\mathbf{r} - \mathbf{u}$ constitutes second order curve(s). For the case of $\mathbf{u} = 0$ the locus is two curves which pass through the FOE and the AOR (and FOC and $-$AOR). The four zero motion contours C_1 to C_4 displayed are defined by the same direction of translation (**t**) and different directions of rotation (ω), with the angle $\alpha = \angle \mathbf{t}\omega$ increasing in value from C_1 to C_4. In (a) and (b) for C_1 and C_2 we have $\alpha < 90^\circ$, in (c) for C_3 $\alpha = 90^\circ$, and in (d) for C_4 $\alpha > 90^\circ$.

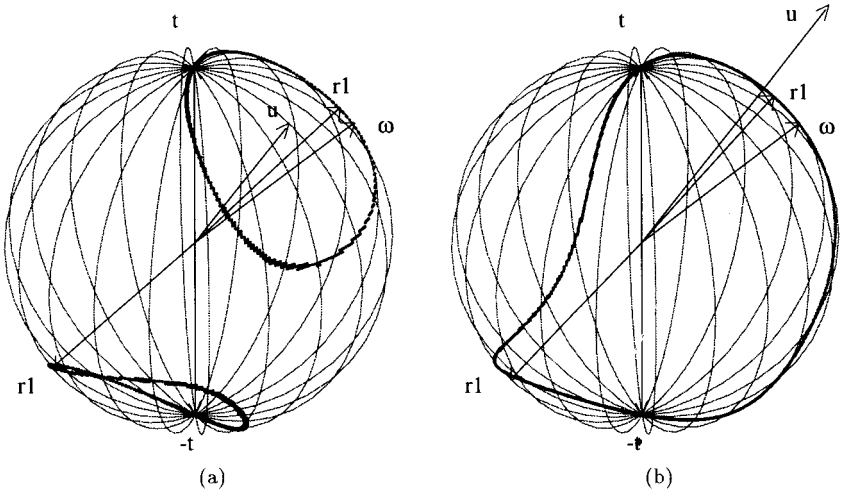

Figure 32. General **u** iso-motion contours pass through the FOE, the FOC, and the points $\mathbf{R}_\mathbf{u}$—the points where the rotational component of the motion is equal to $(\mathbf{u} \cdot \mathbf{r})\mathbf{r} - \mathbf{u}$. The curves displayed in (a) and (b) are defined by the same **t** and ω and parallel vectors **u**.

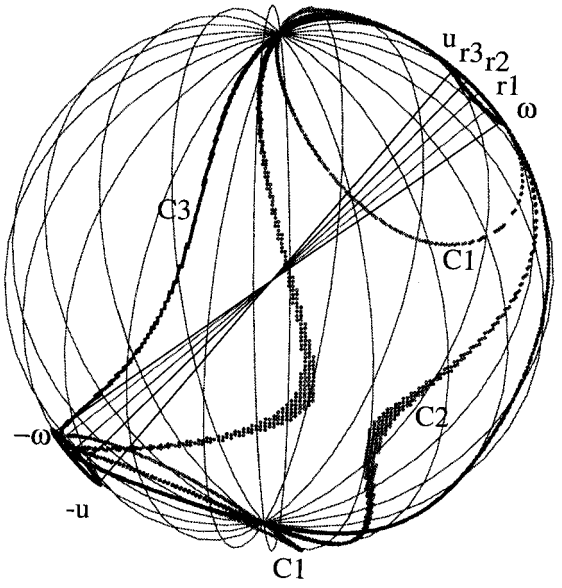

Figure 33. The points $\mathbf{R_u}$ ($\mathbf{r}_1$, $\mathbf{r}_2$, $\mathbf{r}_3$) on $k\mathbf{u}$ iso-motion contours (C_1, C_2, C_3) lie on two curves (small dark curves) described by a second order equation and contain the points $\mathbf{u}$, $-\mathbf{u}$, ω and $-\omega$.

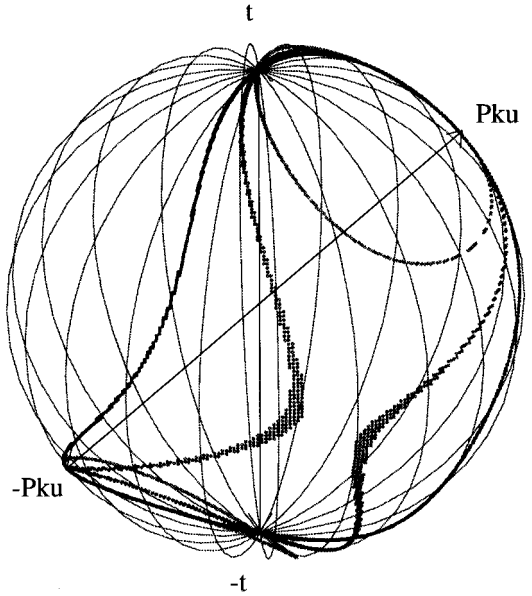

Figure 34. For the general case all $k\mathbf{u}$ iso-motion contours intersect in four points; the FOE, the FOC, and the points $\mathbf{P}_{k\mathbf{u}}$ and $-\mathbf{P}_{k\mathbf{u}}$.

describes the $\mathbf{u}$ iso-motion contours for the $k_i\mathbf{u}$ and $k_j\mathbf{u}$ iso-motion contours, we obtain

$$\mathbf{r} \cdot (\mathbf{u} \times \mathbf{t}) = 0.$$

The above equation describes a great circle independent of k_i and k_j. Thus all $k\mathbf{u}$ iso-motion contours intersect in the same points. These points—in the general case four—are obtained by intersecting the great circle with any iso-motion contour, for example the zero-motion contour. As can be verified through substitution the FOE, the FOC, $\mathbf{P}_{k\mathbf{u}}$, and $-\mathbf{P}_{k\mathbf{u}}$ lie on both the great circle and the zero-motion contour. □

If $(\mathbf{u} \times \mathbf{t}) = 0$ (or $\mathbf{u}$ parallel to $\mathbf{t}$) all the $k\mathbf{u}$ iso-motion contours are the same. If $(\mathbf{t} \times \boldsymbol{\omega}) = 0$ ($\mathbf{t}$ parallel to $\boldsymbol{\omega}$) $\mathbf{P}_{k\mathbf{u}}$ becomes the FOE, and we only obtain two intersection points.

It follows from Theorem 3 that the direction of the motion vector in the intersection points $\mathbf{P}_{k\mathbf{u}}$, and $-\mathbf{P}_{k\mathbf{u}}$ is defined; since these points also lie on the zero-motion contour the vectors $\mathbf{v}$ at the intersection points are parallel to their translational and their rotational motion components.

To obtain on the sphere an analog to the iso-normal motion areas of the plane, the length of the normal motion vector has to be appropriately normalized. Given a 3D vector $\mathbf{u_n}$ (a vector of length u_n and unit vector $\mathbf{n}$) we consider the locus of points $\mathbf{r}$ on the sphere with normal motion vector $\frac{u_n((\mathbf{n}\cdot\mathbf{r})\mathbf{r}-\mathbf{n})}{||(\mathbf{n}\cdot\mathbf{r})\mathbf{r}-\mathbf{n}||^2}$.

Proposition 4. *For a rigid motion field on the sphere and a 3D vector* $\mathbf{u_n}$ *(of length* u_n *and unit vector* $\mathbf{n}$*) the locus of points* $\mathbf{r}$ *on the sphere where the normal motion vector in direction* $(\mathbf{n}\cdot\mathbf{r})\mathbf{r} - \mathbf{n}$ *could take on the value* $\frac{u_n}{||(\mathbf{n}\cdot\mathbf{r})\mathbf{r}-\mathbf{n}||}$ *are areas bounded by a circle and a second order curve* (*see Fig.* 35).

Proof: We have

$$\left(\frac{1}{|\mathbf{R}|}((\mathbf{t}\cdot\mathbf{r})\mathbf{r} - \mathbf{t}) - \boldsymbol{\omega} \times \mathbf{r}\right) \cdot \frac{(\mathbf{n}\cdot\mathbf{r})\mathbf{r} - \mathbf{n}}{||(\mathbf{n}\cdot\mathbf{r})\mathbf{r} - \mathbf{n}||} = \frac{u_n}{||(\mathbf{n}\cdot\mathbf{r})\mathbf{r} - \mathbf{n}||}$$

or

$$\frac{1}{|\mathbf{R}|}((\mathbf{n}\cdot\mathbf{t}) - (\mathbf{t}\cdot\mathbf{r})(\mathbf{r}\cdot\mathbf{n})) = u_n - \mathbf{r}\cdot(\mathbf{n}\times\boldsymbol{\omega})$$

Since $|\mathbf{R}| > 0$ it follows:

$$(\mathbf{n}\cdot\mathbf{t} - (\mathbf{n}\cdot\mathbf{r})(\mathbf{r}\cdot\mathbf{t}))(u_n - \mathbf{r}\cdot(\mathbf{n}\times\boldsymbol{\omega})) > 0$$

The proof follows by the fact that:

(a) The term $\mathbf{n}\cdot\mathbf{t} - (\mathbf{n}\cdot\mathbf{r})(\mathbf{r}\cdot\mathbf{t}) = 0$ describes a second order curve passing from the points where $\mathbf{t}$ and $\mathbf{n}$ pierce the sphere similar to the ones of Fig. 31.

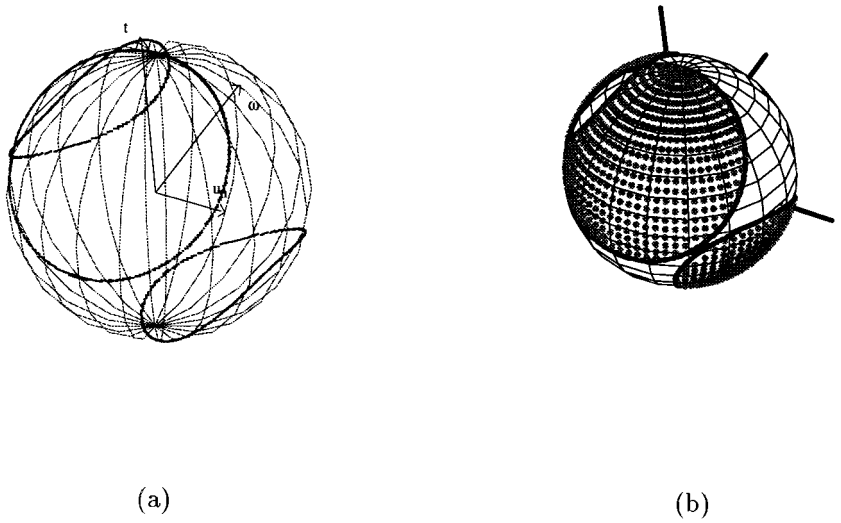

Figure 35. Iso-normal motion areas on the sphere are defined by a second order curve and a circle. (a) Shows the boundaries of the iso-normal motion regions defined by the vectors **t**, ω and $\mathbf{u_n}$ of length 1, 1 and 0.5, where all parts of the sphere (visible and hidden ones are rendered). (b) shows the corresponding iso-normal areas (filled with grey dots) and the directions of the defining vectors with only the visible parts displayed.

(b) The term $u_n - \mathbf{r} \cdot (\mathbf{n} \times \boldsymbol{\omega}) = 0$ describes a circle. When $u_n = 0$ this equation represents a great circle passing through the *AOR* and $-$*AOR*. □

Acknowledgments

The support of ONR and NSF is gratefully acknowledged. Part of this work was done while the authors were visiting NADA, KTH. The support of NUTEK is gratefully acknowledged. Special thanks to Sara Larson for her editorial and graphics assistance.

References

Aloimonos, J. and Brown, C.M. 1984. Direct processing of curvilinear sensor motion from a sequence of perspective images. In *Proc. Workshop on Computer Vision: Representation and Control*, pp. 72–77.

Aloimonos, J.(Y.) 1990. Purposive and qualitative active vision. In *Proc. DARPA Image Understanding Workshop*, pp. 816–828.

Anandan, P. and Weiss, R. 1985. Introducing a smoothness constraint in a matching approach for the computation of optical flow fields. In *Proc. 3rd Workshop on Computer Vision: Representation and Control*, pp. 186–194.

Bergholm, F. 1988. Motion from flow along contours: A note on robustness and ambiguous cases. *International Journal of Computer Vision*, 3:395–415.

Daniilidis, K. 1992. On the error sensitivity in the recovery of object descriptions. Ph.D. Thesis, Department of Informatics, University of Karlsruhe, Germany, in German.

Daniilidis, K. and Nagel, H.H. 1990. Analytical results on error sensitivity of motion estimation from two views. *Image and Vision Computing*, 8:297–303.

Faugeras, O. 1992. *Three Dimensional Computer Vision*. MIT Press, Cambridge, MA.

Faugeras, O.D., Lustman, F., and Toscani, G. 1987. Motion and structure from motion from point and line matches. In *Proc. International Conference on Computer Vision*, pp. 25–34.

Faugeras, O.D. and Maybank, S. 1990. Motion from point matches: Multiplicity of solutions. *International Journal of Computer Vision*, 4:225–246.

Faugeras, O.D. and Papadopoulo, T. 1993. A theory of the motion fields of curves. *International Journal of Computer Vision*, 10(2):125–156.

Fermüller C. 1993. Navigational preliminaries. In *Active Perception, Advances in Computer Vision*, Y. Aloimonos (Ed.). Lawrence Erlbaum: Hillsdale, NJ.

Fermüller, C. and Aloimonos, Y. 1995. Qualitative egomotion. *International Journal of Computer Vision*, 15:7–29.

Fermüller, C. and Aloimonos, Y. 1993. The role of fixation in visual motion analysis. *International Journal of Computer Vision: Special Issue on Active Vision*, M. Swain (Ed.), 11(2):165–186.

Fernmüller, C. and Aloimonos, Y. 1996. Direct motion perception. In *Visual Navigation*: *From Biological Systems to Unmanned Ground Vehicles*, *Advances in Computer Vision*, Y. Aloimonos (Ed.). Lawrence Erlbaum, Hillsdale, NJ.

Gårding, J., Porrill, J., Mayhew, J.E.W., and Frisby, J.P. 1993. Binocular stereopsis, vertical disparity and relief transformations. Technical Report TRITA-NA-P9334, CVAP, Royal Institute of Technology, Stockholm, Sweden.

von Helmholtz, H. 1896. *Handbuch der Physiologischen Optik*. Leopold Voss.

Hildreth, E. 1984. Computations underlying the measurement of visual motion. *Artificial Intelligence*, 23:309–354.

Horn, B.K.P. 1990. Relative orientation. *International Journal of Computer Vision*, 4:59–78.

Horn, B.K.P. and Schunck, B. 1981. Determining optical flow. *Artificial Intelligence*, 17:185–203.

Horn, B.K.P. and Weldon, E.J. 1987. Computationally efficient methods for recovering translational motion. In *Proc. International Conference on Computer Vision*, pp. 2–11.

Jain, R. 1983. Direct computation of the focus of expansion. *IEEE Transactions on Pattern Analysis and Machine Intelligence*, 5:58–64.

Koenderink, J.J. 1986. Optic flow. *Vision Research*, 26:161–180.

Koenderink, J.J. and van Doorn, A.J. 1991. Affine structure from motion. *Journal of the Optical Society of America*, 8:377–385.

Liu, Y. and Huang, T.S. 1988. Estimation of rigid body motion using straight line correspondences. *Computer Vision, Graphics, and Image Processing*, 43:37–52.

Longuet-Higgins, H.C. and Prazdny K. 1980. The interpretation of a moving retinal image. *Proceedings of the Royal Society*, London B, 208:385–397.

Maybank, S. 1993. *Theory of Reconstruction from Image Motion*. Springer: Berlin, Heidelberg.

Navab, N., Faugeras, O.D., and Vieville, T. 1993. The critical sets of lines for camera displacement estimation: A mixed euclidian-protective and constructive approach. In *Proc. International Conference on Computer Vision*, pp. 713–723.

Nelson, R.C. and Aloimonos, J. 1988. Finding motion parameters from spherical flow fields (or the advantage of having eyes in the back of your head). *Biological Cybernetics*, 58:261–273.

Prazdny, K. 1980. Egomotion and relative depth map from optical flow. *Biological Cybernetics*, 36:87–102.

Selby, S.M. (Ed.) 1972. *Standard Mathematical Tables*, Chemical Rubber Co.: Cleveland, Ohio.

Shulman, D. and Hervé, J.-Y. 1989. Regularization of discontinuous flow fields. In *Proc. IEEE Workshop on Visual Motion*, pp. 81–86.

Spetsakis, M.E. and Aloimonos, J. 1988. Optimal computing of structure from motion using point correspondence. In *Proc. International Conference on Computer Vision*, pp. 449–453.

Tistarelli, M. and Sandini, G. 1992. Dynamic aspects in active vision. *CVGIP: Image Understanding: Special Issue on Purposive*, Y. Aloimonos (Ed.) *Qualitative, Active Vision*, 56:108–129.

Tsai, R.Y. and Huang, T.S. 1984. Uniqueness and estimation of three-dimensional motion parameters of rigid objects with curved surfaces. *IEEE Transactions on Pattern Analysis and Machine Intelligence*, 6:13–27.

Ullman, S. 1979. *The Interpretation of Visual Motion*. MIT Press.

Ullman, S. and Basri, R. 1991. Recognition by linear combination of models. *IEEE Transactions on Pattern Analysis and Machine Intelligence*, 13:992–1006.

Verri, A. and Poggio, T. 1989. Motion field and optical flow: Qualitative properties. *IEEE Transactions on Pattern Analysis and Machine Intelligence*, 11:490–498.